BIOCHEMISTRY
including biophysical chemistry & molecular biology

Article

pubs.acs.org/biochemistry

Open Access on 06/08/2015

Molecular Basis of Gain-of-Function LEOPARD Syndrome-Associated SHP2 Mutations

Zhi-Hong Yu,[†] Ruo-Yu Zhang,[†] Chad D. Walls,[†] Lan Chen,[†,‡] Sheng Zhang,[†,‡] Li Wu,[†,‡] Sijiu Liu,[†] and Zhong-Yin Zhang*[,†]

[†]Department of Biochemistry and Molecular Biology, Indiana University School of Medicine, 635 Barnhill Drive, Indianapolis, Indiana 46202, United States

[‡]Chemical Genomics Core Facility, Indiana University School of Medicine, 635 Barnhill Drive, Indianapolis, Indiana 46202, United States

ABSTRACT: The Src homology 2 (SH2) domain-containing protein tyrosine phosphatase 2 (SHP2) is a critical signal transducer downstream of growth factors that promotes the activation of the RAS-ERK1/2 cascade. In its basal state, SHP2 exists in an autoinhibited closed conformation because of an intramolecular interaction between its N-SH2 and protein tyrosine phosphatase (PTP) domains. Binding to pTyr ligands present on growth factor receptors and adaptor proteins with its N-SH2 domain localizes SHP2 to its substrates and frees the active site from allosteric inhibition. Germline mutations in SHP2 are known to cause both Noonan syndrome (NS) and LEOPARD syndrome (LS), two clinically similar autosomal dominant developmental disorders. NS-associated SHP2 mutants display elevated phosphatase activity, while LS-associated SHP2 mutants exhibit reduced catalytic activity. A conundrum in how clinically similar diseases result from mutations to SHP2 that have opposite effects on this enzyme's catalytic functionality exists. Here we report a comprehensive investigation of the kinetic, structural, dynamic, and biochemical signaling properties of the wild type as well as all reported LS-associated SHP2 mutants. The results reveal that LS-causing mutations not only affect SHP2 phosphatase activity but also induce a weakening of the intramolecular interaction between the N-SH2 and PTP domains, leading to mutants that are more readily activated by competing pTyr ligands. Our data also indicate that the residual phosphatase activity associated with the LS SHP2 mutant is required for enhanced ERK1/2 activation. Consequently, catalytically impaired SHP2 mutants could display gain-of-function properties because of their ability to localize to the vicinity of substrates for longer periods of time, thereby affording the opportunity for prolonged substrate turnover and sustained RAS-ERK1/2 activation.

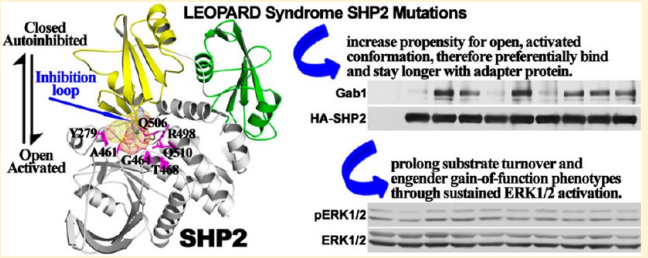

The proper level of protein tyrosine phosphorylation, maintained by the coordinated and reciprocal activities of protein tyrosine kinases (PTKs) and protein tyrosine phosphatases (PTPs), is important for the regulation of signaling pathways that control various developmental processes as well as cell growth, differentiation, metabolism, motility, and survival.[1,2] Not surprisingly, perturbation of the delicate balance between the actions of PTKs and PTPs often leads to abnormal tyrosine phosphorylation, which is responsible for the pathogenesis of many human diseases, including cancer, diabetes/obesity, and autoimmune disorders.[1,3−5] By catalyzing the removal of phosphate from tyrosine, PTPs are usually perceived as negative regulators of cell signaling, which is often driven by tyrosine phosphorylation-mediated events. Interestingly, the Src homology 2 (SH2) domain containing protein tyrosine phosphatase 2 (SHP2), encoded by *Ptpn11*, has been shown to play a positive role in signal transduction.[6−8] Genetic and biochemical studies reveal that SHP2 acts downstream of growth factor and cytokine receptors and upstream of RAS, a critical node in many signaling pathways that underlies growth factor/cytokine-induced cell proliferation, migration, and survival.[9−12] Importantly, SHP2's phosphatase activity is required for activation of the RAS-ERK1/2 (extracellular signal-regulated kinase 1 and 2) pathway.[6,13]

SHP2 consists of two tandem SH2 domains at its N-terminus, a PTP domain in the middle, and a C-terminal tail. SHP2 is an allosteric enzyme whose phosphatase activity is regulated by an elegant "molecular switch" mechanism.[14,15] In its basal state, SHP2 is autoinhibited because of an intramolecular interaction between its N-SH2 and PTP domains, which blocks the entrance of the substrate to the active site.[14,16] Upon growth factor or cytokine stimulation, the N-SH2 domain binds tyrosine-phosphorylated sequence motifs in receptor tyrosine kinases, cytokine receptors, or more commonly scaffold proteins, which localize SHP2 to the vicinity of its substrates and simultaneously weaken the N-SH2

Received: March 4, 2014
Revised: June 7, 2014
Published: June 8, 2014

   dx.doi.org/10.1021/bi5002695 | *Biochemistry* 2014, 53, 4136−4151

domain−PTP domain interaction, liberating the PTP domain to catalyze substrate turnover.[17,18]

The importance of SHP2 to human health is supported by genetic observations linking SHP2 mutations to several pathological conditions. Somatic activating mutations in SHP2 are associated with various types of leukemia[19,20] and solid tumors.[21−23] Germline SHP2 mutations cause autosomal dominant developmental disorders, including 50 and 90% of documented Noonan syndrome (NS) and LEOPARD (an acronym for its clinical features of multiple lentigines, electrocardiographic conduction abnormalities, ocular hypertelorism, pulmonic stenosis, abnormalities of genitalia, retardation of growth, and deafness) syndrome (LS) cases, respectively.[24−27] Other than the presence of multiple lentigines, which is a hallmark of LS, NS and LS share similar clinical features such as short stature, craniofacial malformations, and congenital heart abnormalities.

More than 40 NS-associated SHP2 mutations have been described, affecting 30 different residues located in or close to the N-SH2 domain−PTP domain interface.[21,22] In general, NS-associated SHP2 mutants display gain-of-function (GOF) phenotypes with heightened RAS-ERK1/2 pathway activation, likely because of elevated phosphatase activity caused by disruption of the autoinhibitory interaction between the N-SH2 and PTP domains.[28−33] By contrast, 11 LS-associated SHP2 mutations that alter seven different residues, all residing in the PTP domain, have been identified. Unlike NS mutants, the LS-associated SHP2 mutants are reported to exhibit reduced phosphatase activity and are deemed loss-of-function (LOF) variants.[32,34,35] An obvious unresolved question is how mutations that incite opposite effects on SHP2 phosphatase activity elicit overlapping disease phenotypes. To address this question, we postulated that disease-causing SHP2 mutations affect not only SHP2 phosphatase activity but also its molecular switching mechanism, and thus, detailed comparative analysis of the structure and function of wild-type and mutant SHP2 enzymes will yield insight into the biochemical basis that underlies the pathological processes potentiated by the mutant enzymes. Our initial investigation of the most recurrent LS-associated SHP2 mutant Y279C revealed that although Y279C is catalytically impaired and exists in a closed conformation, the Y279C mutation weakens the interaction between the N-SH2 and PTP domains.[36] The weakened interaction between the two domains in Y279C results in an increased level of binding between the N-SH2 domain and its pTyr ligands. Consequently, Y279C stays longer with the scaffolding protein Gab1, thus prolonging substrate turnover, which compensates for the reduced phosphatase activity, leading to sustained RAS-ERK1/2 activation. Collectively, the data show that although the Y279C mutant has a lower catalytic activity, the mutation also perturbs the "molecular switch" mechanism of SHP2 to engender a GOF phenotype. However, given the diverse nature of the reported LS SHP2 mutations, it is essential to determine if these LS-associated SHP2 mutations similarly contribute to the pathogenesis of LS in the same manner as the Y279C mutant. This is an important issue, because the structural requirement and substrate specificity of LS-associated SHP2 mutants could be different from each other; thus, targeting SHP2 in LS may require different strategies. Herein, we describe a detailed structural and mechanistic characterization of the LS-associated SHP2 mutants (Y279C, A461T, G464A, T468M, R498L, Q506P, and Q510E) covering all seven known LS mutation sites.

MATERIALS AND METHODS

Cloning, Expression, and Purification of Proteins. The SHP2 wild-type catalytic domain (CD, residues 224−528), the full-length lacking the C-terminal tail (FL, residues 1−528), and the N-SH2 domain (residues 4−103) were cloned into the pET-21a+ vector using NdeI and XhoI restriction enzymes (NEB), which generated recombinant proteins with a C-terminal six-His tag. The SHP2 catalytic domains and full-length constructs lacking the C-terminal tail containing individual LS mutations (Y279C, A461T, G464A, T468M, R498L, Q506P, and Q510E) were generated using the QuikChange mutagenesis kit (Stratagene). All proteins were expressed in *Escherichia coli* BL21(DE3). Proteins used for kinetic or inhibition assays were purified using Ni-NTA resin (Qiagen); the purities were >90% as determined by sodium dodecyl sulfate−polyacrylamide gel electrophoresis (SDS−PAGE) and Coomassie staining. Proteins used for crystallography studies were first purified with Ni-NTA resin, followed by sequential chromatography with a HiPrep 26 desalting column (GE Healthcare), a cation exchange column packed with SP Sepharose (GE Healthcare), and a Superdex 75 gel filtration column (GE Healthcare). The purities were >95% as determined by SDS−PAGE and Coomassie staining.

Enzyme Kinetic Analysis of Wild-Type SHP2 and Its LS Mutants. Initial rate measurements for the enzyme-catalyzed hydrolysis of *p*-nitrophenyl phosphate (*p*NPP) were conducted at 25 °C in a pH 7.0 assay buffer (50 mM 3,3-dimethylglutarate, 1 mM DTT, 1 mM EDTA, and 150 mM NaCl). The assays were performed in 96-well plates in a total reaction volume of 200 μL. Substrate concentrations ranging from $0.2K_m$ to $5K_m$ were used to determine k_{cat} and K_m. Reactions were started by the addition of an appropriate amount of enzyme to a 100 μL *p*NPP solution. The reactions were quenched with 50 μL of 5 M sodium hydroxide, and the absorbance at 405 nm was detected using a SpectraMax Plus 384 microplate spectrophotometer (Molecular Devices). The steady-state kinetic parameters were determined by fitting the data to the Michaelis−Menten equation in SigmaPlot.

To determine the k_{cat}/K_m for pTyr-containing peptide substrates, the reaction (0.5 mL) was conducted in a 1 mL quartz cuvette at 25 °C in pH 7.0 assay buffer (50 mM 3,3-dimethylglutarate, 1 mM DTT, 1 mM EDTA, and 150 mM NaCl). The reaction rate was monitored by the increase in fluorescence of the dephosphorylated peptide product at 305 nm with excitation at 280 nm on a PerkinElmer model LS50B luminescence spectrometer.[37] The reaction was performed at a substrate concentration much lower than its K_m, and the enzyme concentration was at least 10 times lower than the substrate concentration. Under this condition, the Michaelis−Menten equation reduces to the equation $v = (k_{cat}/K_m)[E][S]$. The reaction is first-order with respect to [S], and the observed apparent first-order rate constant is equal to $(k_{cat}/K_m)[E]$, which can be determined by fitting the reaction time course data to a first-order rate equation in SigmaPlot. The k_{cat}/K_m value is calculated from the first-order rate constant divided by a given enzyme concentration.

Assay of the Inhibition of the SHP2 PTP Domain by the N-SH2 Domain. PTP activity was assayed using *p*NPP as a substrate at 25 °C in pH 7.0 assay buffer (50 mM 3,3-dimethylglutarate, 1 mM DTT, 1 mM EDTA, and 150 mM NaCl). The assays were performed in 96-well plates in a total reaction volume of 200 μL. The reaction was initiated by the

dx.doi.org/10.1021/bi5002695 | *Biochemistry* 2014, 53, 4136−4151

addition of enzyme (wild-type SHP2 or the LS SHP2 mutant catalytic domain) to a reaction mixture containing *p*NPP and the isolated SHP2 N-SH2 domain. For the determination of K_i, the *p*NPP concentration was varied at three different concentrations of the N-SH2 domain. The reaction rate was measured using a SpectraMax Plus 384 microplate spectrophotometer (Molecular Devices). The K_i values were determined by fitting the data using the EnzymeKinetics module in SigmaPlot.

Crystallization, Data Collection, and Structure Determination. All crystals were grown at 20 °C in hanging drops containing 1.5 μL of a protein solution with 1.5 μL of a reservoir solution. Proteins were dissolved in a pH 7.8 Tris buffer containing 20 mM Tris-HCl, 50 mM NaCl, 2 mM DTT, and 1 mM EDTA. The reservoir solution and protein concentration were optimized to yield high-quality crystals for different LS SHP2 mutants, for example, 18% PEG3350 and 300 mM KF for A461T (10 mg/mL), 20% PEG3350 and 300 mM LiCl for G464A (8 mg/mL), 20% PEG3350 and 300 mM KCOOH for T468M (8 mg/mL), 20% PEG3350 and 200 mM KF for Q506P (8 mg/mL), and 18% PEG3350 and 200 mM KF for Q510E (10 mg/mL). The crystals were transferred into the cryoprotectant buffer, containing the same components in the reservoir solution except with an increased concentration of PEG3350 (30%), and were flash-frozen with liquid nitrogen. Data were collected at beamline 19-BM (for T468M and A461T) or 19-ID (for G464A, Q506P, and Q510E) at the Advanced Photon Source (APS) and were processed with HKL3000.[38] The structures were determined by molecular replacement with Molrep[39] using the coordinates of our previously reported SHP2 wild-type structure [Protein Data Bank (PDB) entry 4DGP][36] as a search model. The structural refinements were conducted iteratively using the phenix.refine program in the PHENIX software suite.[40]

Hydrogen/Deuterium Exchange Mass Spectrometry. Stock solutions of wild-type SHP2 and its mutants (residues 1−528) were prepared in a ^1H_2O-based buffer (pH 7.8). Deuterium exchange was initiated by 20-fold dilution of each enzyme in a similar deuterium ^2H_2O buffer (pD 7.8). At set deuterium exchange time points (10 s, 30 s, 1 min, 10 min, 30 min, and 60 min), the reaction was quenched by the addition of a cold ^1H_2O-based 100 mM sodium phosphate buffer (pH 2.3) at equal volume. For peptide-based mass spectrometry analysis, the quench solution contained pepsin endoproteinase (Sigma) that would make a pepsin:SHP2 ratio of 1.5:1 (w:w) during digestion. The quenched sample was digested on ice for 4 min and then loaded via an autosampler onto an XBridge C18 2.5 μm, 2.1 mm × 50 mm (Waters) column that was submerged in ice. A Surveyor MS pump (Finnigan) was used to generate the chromatographic gradients. Peptides were separated over time using a steep gradient of acetonitrile (10 to 35% over 7.5 min) and electrosprayed into an LTQ mass spectrometer (Finnigan). Sequest (Thermo) was used to identify SHP2 peptic peptides. Peptides were accepted for analysis on the basis of XCorr value significance and identification in multiple sample runs. All peptide-based samples were manually prepared and run in triplicate with a general standard deviation of <0.2 Da per time point. Unbiased peptide precursor ion peak envelope centroiding was performed using HX-express.[41] Significant deuterium exchange differences in SHP2 mutants relative to WT were mapped onto the SHP2 sequence and crystal structure in a heat map format.

Cell Culture, Immunoblotting, and Immunoprecipitation. HEK293 cells were cultured at 37 °C and 5% CO_2 in Dulbecco's modified Eagle's medium (Invitrogen) supplemented with 10% fetal bovine serum (HyClone). The WT or SHP2 mutant (E76K, Y279C, A461T, G464A, T468M, R498L, Q506P, Q510E, C459S, and Y279C/C459S) cloned in mammalian expression vector pCN-HA, a modified version of pcDNA3.1 that generated proteins with an N-terminal HA tag, was transfected into HEK293 cells using Lipofectamine 2000 (Invitrogen) according to the manufacturer's instructions. Twenty-four hours post-transfection, cells were serum-starved overnight and then either left unstimulated or stimulated with EGF (5 or 50 ng/mL) or 10 ng/mL HGF for various periods of time (0, 30, and 60 min). All growth factors were obtained from Sigma. For immunoblotting, the cell lysates were electrophoresed on a 10% polyacrylamide gel and the separated proteins were transferred to a nitrocellulose membrane and probed with anti-phospho-ERK1/2 (Cell Signaling), anti-ERK1/2 (Cell Signaling), anti-Phospho-Paxillin (Tyr118) (Cell Signaling), anti-Paxilin (BD Transduction Laboratories), anti-HA (Santa Cruz), and anti-GAPDH (Santa Cruz) antibodies followed by incubation with horseradish peroxidase-conjugated secondary antibodies. The blots were developed by the enhanced chemiluminescence technique using the SuperSignal West Pico Chemiluminescent substrate (Pierce). For immunoprecipitation, the cells were lysed on ice for 30 min in lysis buffer [50 mM Tris-HCl (pH 7.4), 150 mM NaCl, 1% Triton X-100, 10% glycerol, 10 mM NaF, and 1 mM $NaVO_4$] supplemented with a complete protease inhibitor tablet (Roche). Cell lysates were cleared by centrifugation at 15000 rpm for 20 min. The lysate protein concentration was estimated using a BCA protein assay kit (Pierce). Three micrograms of HA antibody (Santa Cruz) was added to 1 mg of cell lysate and incubated at 4 °C for 3 h with protein A/G-agarose beads (Santa Cruz). After being washed three times with lysis buffer, the protein complex was boiled with Laemmli sample buffer and subjected to electrophoresis and immunoblotting. Representative results from at least two independent experiments are shown.

RESULTS

LS-Associated SHP2 Mutants Exhibit Reduced Catalytic Activity. On the basis of their locations in the PTP domain, it has been suggested that LS SHP2 mutations may harm SHP2 phosphatase activity. Previous studies were limited to immunoprecipitated enzymes and/or substrates, and activity measurements were conducted at a single substrate concentration. We set out to determine the kinetic parameters for wild-type SHP2 and LS SHP2 mutant-catalyzed reactions using both a small molecule chromogenic substrate *p*NPP and pTyr-containing peptides as substrates. To conduct rigorous kinetic measurements, we expressed and purified the recombinant SHP2 catalytic domain (CD, residues 224−528) and full-length construct lacking the C-terminal tail (FL, residues 1−528) for the wild type and seven LS mutants (Y279C, A461T, G464A, T468M, R498L, Q506P, and Q510E). Previous studies have shown that truncation of the C-terminus does not affect the autoinhibition mechanism.[14] Kinetic parameters for the enzyme-catalyzed reaction were determined at pH 7.0 and 25 °C. Because *p*NPP is a small aryl phosphate that mimics pTyr, its hydrolysis is sensitive only to structural perturbations to the active site. Thus, results with *p*NPP will reveal the effects of LS SHP2 mutations on the intrinsic phosphatase activity of SHP2.

Table 1. Kinetic Parameters of Wild-Type SHP2 and Its Mutants with *p*NPP as a Substrate

	CD (224−528)		FL (1−528)		fold of autoinhibition	
enzyme	k_{cat} (s^{-1})	K_m (mM)	k_{cat} (s^{-1})	K_m (mM)	(CD/FL)k_{cat}	(CD/FL)k_{cat}/K_m
WT	6.5 ± 0.3	4.3 ± 0.5	0.13 ± 0.02	3.4 ± 0.5	50	40
Y279C	0.56 ± 0.13	17.7 ± 1.3	0.025 ± 0.006	7.0 ± 0.7	22	9
A461T	0.0070 ± 0.0009	6.0 ± 0.6	0.0023 ± 0.0001	2.2 ± 0.1	3	1
G464A	0.071 ± 0.012	3.9 ± 0.2	0.018 ± 0.004	2.6 ± 0.3	4	3
T468M	0.090 ± 0.016	3.1 ± 0.5	0.0034 ± 0.0004	3.0 ± 0.2	26	26
R498L	0.038 ± 0.001	8.4 ± 0.4	0.039 ± 0.001	5.9 ± 0.1	1	1
Q506P	0.64 ± 0.11	4.5 ± 0.4	0.055 ± 0.016	2.4 ± 0.3	12	6
Q510E	0.033 ± 0.006	8.6 ± 0.9	0.017 ± 0.001	2.8 ± 0.1	2	1

Table 2. k_{cat}/K_m Values ($\times 10^{-3}$ M^{-1} s^{-1}) of Wild-Type SHP2 and Its Mutants with pTyr Peptides as Substrates and Fold Autoinhibition Defined by (CD/FL)k_{cat}/K_m

enzyme	Sprouty1/pY53	Paxillin/pY118	EGFR/pY992	Gab1/pY589
WT/CD	110 ± 0.9	123 ± 1.0	1167 ± 23	60 ± 0.7
WT/FL	5.1 ± 0.1	5.2 ± 0.2	95 ± 1.4	3.0 ± 0.07
fold autoinhibition	22	24	12	20
Y279C/CD	0.2 ± 0.004	0.08 ± 0.001	2.3 ± 0.01	0.1 ± 0.001
Y279C/FL	0.06 ± 0.003	0.04 ± 0.001	0.4 ± 0.003	0.04 ± 0.001
fold autoinhibition	3	2	6	3
T468M/CD	3.8 ± 0.06	4.2 ± 0.07	52 ± 1	1.6 ± 0.02
T468M/FL	0.08 ± 0.003	0.18 ± 0.008	3.53 ± 0.01	0.12 ± 0.002
fold autoinhibition	48	23	15	13

Table 3. Data Collection and Structural Refinement Statistics[a]

	A461T	G464A	T468M	Q506P	Q510E
			Data Collection		
space group	$P2_12_12$	$P2_12_12$	$P2_1$	$P2_12_12$	$P2_12_12$
cell dimensions					
a (Å)	54.3	55.5	45.3	54.5	55.3
b (Å)	206.7	204.9	209.3	222.2	219.2
c (Å)	41.9	44.5	56.1	40.9	41.7
α, β, γ (deg)	90.0, 90.0, 90.0	90.0, 90.0, 90.0	90.0, 95.9, 90.0	90.0, 90.0, 90.0	90.0, 90.0, 90.0
resolution (Å)	2.7	2.5	2.4	2.7	2.2
total no. of observations	68055	103779	142433	75697	119547
no. of unique observations	13063	17946	38926	14319	26886
completeness (%)	94.9 (74.1)	99.7 (99.9)	94.4 (73.1)	98.7 (96.3)	98.2 (92.7)
redundancy	5.2 (3.1)	5.8 (5.6)	3.7 (2.4)	5.3 (5.1)	4.4 (4.0)
$\langle I \rangle/\sigma$	18.7 (4.2)	14.9 (1.9)	22.6 (1.9)	17.6 (1.7)	13.6 (1.6)
R_{merge} (%)	12.2 (30.9)	16.1 (68.2)	8.5 (64.9)	13.8 (70.9)	13.5 (73.3)
			Structural Refinement		
resolution (Å)	2.7	2.5	2.4	2.7	2.2
no. of reflections	12985	17776	38210	14196	26094
R_{work}/R_{free} (%)	20.2/27.1	18.7/25.6	19.1/25.9	20.3/26.6	20.8/26.2
no. of atoms					
protein	3996	3956	7824	3984	4039
water	55	131	330	55	219
B factor					
protein	43.2	41.9	41.8	59.9	38.7
water	34.2	38.2	42.3	47.8	38.5
rmsd					
bond lengths (Å)	0.009	0.008	0.008	0.009	0.008
bond angles (deg)	1.186	1.068	1.129	1.182	1.075
Ramachandran plot (%)					
favored	91.9	95.6	94.3	93.8	95.3
allowed	7.2	3.3	4.9	5.4	4.5
disallowed	0.8	1.0	0.8	0.8	0.2

[a]Each data set was collected from a single crystal. Values in parentheses are for the highest-resolution shell.

dx.doi.org/10.1021/bi5002695 | *Biochemistry* 2014, 53, 4136−4151

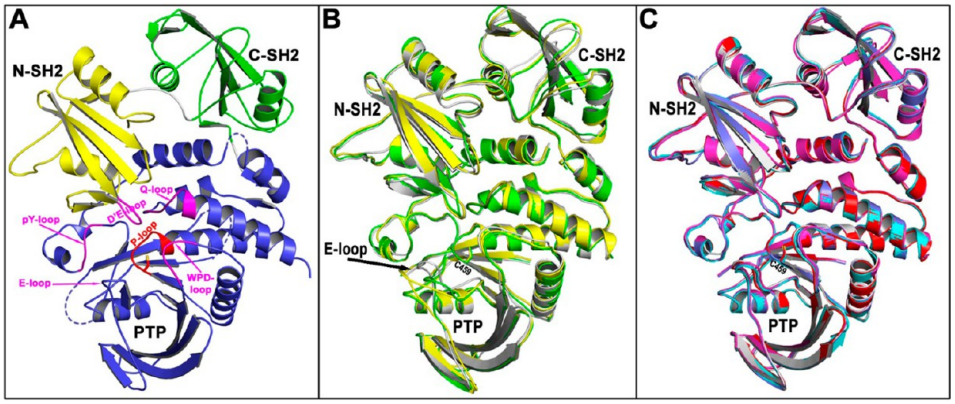

Figure 1. Overall structures of wild-type SHP2 and six LS SHP2 mutants. (A) Closed conformation of SHP2 represented by the wild-type crystal structure. N-SH2, C-SH2, and PTP domains are colored yellow, green, and blue, respectively. The D′E-loop in the N-SH2 domain and five loop fragments (P-loop, pY-loop, WPD-loop, Q-loop, and E-loop) constituting the active pocket in the PTP domain are highlighted. (B) Structural superimposition of A461T (yellow) and G464A (green) on wild-type SHP2 (gray). (C) Structural superimposition of Y279C (cyan), T468M (purple), Q506P (blue), and Q510E (red) on wild-type SHP2 (gray).

As shown in Table 1, the k_{cat} of full-length SHP2 is only 2% of that of the catalytic domain, which is consistent with the structural finding that full-length SHP2 is in an autoinhibited, closed conformation.[14,36] The phosphatase activities of the LS SHP2 mutant catalytic domains are lower than those of the wild-type SHP2 counterpart, ranging from 10-fold (Q506P) to 930-fold (A461T). Interestingly, with the exception of R498L, the k_{cat} values of the full-length LS SHP2 mutants are still 2−26-fold lower than those of their corresponding catalytic domains. These results suggest that, similar to wild-type SHP2, these full-length LS SHP2 mutants also exist in a closed, autoinhibited conformation. Because the full-length and catalytic domain constructs of R498L exhibit similar activity, R498L may already exist in the open conformation.

To further investigate the effect of LS SHP2 mutations on SHP2 activity, we also utilized more physiologically relevant substrates, i.e., pTyr-containing peptides derived from putative SHP2 substrate proteins, including EGFR/pY992 (DADE-pY^{992}LIPQQG),[42] Sprouty1/pY53 (GSNEpY^{53}TEGPS),[43] Paxillin/pY118 (EEHVpY^{118}SFPN),[44] and Gab1/pY589 (DSEEN-pY^{589}VPMNPNL).[45] These pTyr-containing peptides are supposed to preferentially bind with the catalytic site as substrates, but to minimize potential competition because of binding of the pTyr peptide to the N-SH2 domain, we determined the k_{cat}/K_m value, a measure of substrate specificity, under conditions where substrate concentrations were much lower than K_m. The SHP2-catalyzed dephosphorylation of the pTyr peptides was monitored by the increase in tyrosine fluorescence at pH 7.0 and 25 °C, and k_{cat}/K_m was directly calculated from the reaction progress curve.[37] Table 2 lists the k_{cat}/K_m values for two of the most recurrent LS SHP2 mutants, Y279C and T468M. Similar to results obtained with *p*NPP, the ability of the LS SHP2 mutants to catalyze the hydrolysis of pTyr-containing peptides is significantly compromised. Also, the full-length wild-type and LS SHP2 mutant presumably exist in the autoinhibited state because their k_{cat}/K_m values are considerably lower than those of their corresponding catalytic domains. Finally, the relative preference for the peptide substrates exhibited by the LS SHP2 mutants is similar to that of the wild-type enzyme, indicating that LS SHP2 mutations do not alter SHP2 substrate specificity.

LS SHP2 Mutants Exist in the Closed Conformation, but with Weakened Intramolecular N-SH2−PTP Interdomain Interaction. Given the diverse nature of LS SHP2 mutations, we believe that it is important to obtain three-dimensional structures for all LS SHP2 mutants to fully understand the molecular underpinnings responsible for the disease. Following our previous structural analysis of wild-type SHP2 and LS SHP2 mutant Y279C,[36] we proceeded to determine the crystal structures of the six other LS SHP2 mutants (A461T, G464A, T468M, R498L, Q506P, and Q510E). Similar to earlier studies, the SHP2 constructs (residues 1−528) encompass the two tandem SH2 domains and the PTP domain. We acquired crystals for all LS SHP2 mutants and obtained diffraction data for A461T, G464A, T468M, Q506P, and Q510E, but not R498L. The data collection and structural refinement statistics for the five LS SHP2 mutants are summarized in Table 3. Except for T468M, which crystallized in the $P2_1$ space group with two molecules per asymmetric unit, the other four mutants crystallized in the $P2_12_12$ space group with one molecule per asymmetric unit, similar to wild-type SHP2 and the Y279C LS SHP2 mutant.[36]

To gain structural insight into LS SHP2 mutations, we superimposed the structure of each mutant onto that of wild-type SHP2 (Figure 1) and calculated the root-mean-square deviation (rmsd) of Cα atoms (mutant vs wild type) for the full-length protein, individual domain, or selected loops in SHP2 (Table 4). As already reported,[14,36] wild-type SHP2 is in a closed conformation (Figure 1A): the D′E-loop in the N-SH2

Table 4. rmsd Values (mutant vs wild type, in angstroms) of Cα Atoms Calculated by Superimposing the Mutant Structure onto the Wild-Type SHP2 Structure

	A461T	G464A	Y279C	T468M	Q506P	Q510E
overall	1.33	1.30	0.42	0.72	0.43	0.57
N-SH2 domain	1.16	0.93	0.34	0.66	0.35	0.91
C-SH2 domain	0.46	0.34	0.29	0.43	0.36	0.35
PTP domain	1.12	0.59	0.34	0.42	0.27	0.34
D′E-loop	0.50	0.68	0.20	0.18	0.17	0.17
P-loop	0.26	0.13	0.16	0.18	0.11	0.18
pY-loop	0.20	0.10	0.12	0.13	0.11	0.10
WPD-loop	0.13	0.09	0.07	0.24	0.26	0.14
Q-loop	0.16	0.29	0.13	0.18	0.38	0.15
E-loop	3.73	1.28	0.29	0.21	0.21	0.27

dx.doi.org/10.1021/bi5002695 | *Biochemistry* 2014, 53, 4136−4151

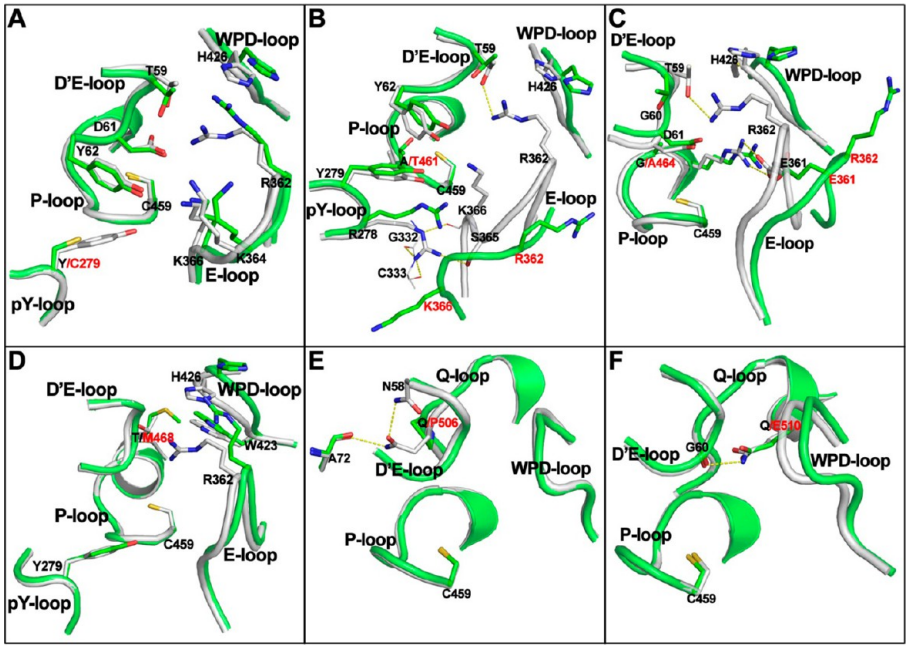

Figure 2. LS SHP2 mutation weakens the N-SH2−PTP interdomain interaction. The weakened interactions are represented by steric and/or electrostatic alterations within mutants (A) Y279C, (B) A461T, (C) G464A, (D) T468M, (E) Q506P, and (F) Q510E. In each panel, wild-type SHP2 is colored gray and the specific LS mutant green. The mutation site is colored red. Polar interactions that existed in the wild type but disappeared in the mutant are denoted with yellow dashed lines.

domain penetrates into the active site pocket walled by five loops (known as the P-loop, pY-loop, WPD-loop, Q-loop, and E-loop) in the PTP domain, physically occluding the active site. In agreement with the prediction from our kinetic experiments, LS SHP2 mutants Y279C, A461T, G464A, T468M, Q506P, and Q510E are indeed found in an autoinhibited, closed conformation. The rmsds for the full-length structures range from 0.418 to 1.332 Å among all six mutants, indicating that the overall structures of the LS SHP2 mutants are similar to that of the wild-type enzyme (Figure 1B,C). Interestingly, LS SHP2 mutations in the P-loop induce the largest structural perturbations, especially among residues in the E-loop (Figure 1B), as evidenced by the relatively higher rmsd values for A461T and G464A (~1.3 Å). Fairly small rmsd values were observed for the other four mutants (Y279C, T468M, Q506P, and Q510E), suggesting that these mutations cause no obvious structural alterations in the overall structures (Figure 1C).

Although Y279C, A461T, G464A, T468M, Q506P, and Q510E are still in the closed conformation, closer comparison of the mutant and wild-type structures reveals that these mutations destabilize the intramolecular N-SH2−PTP interdomain interaction. The Y279C mutation (Figure 2A) abrogates the interaction between the phenol group and the side chains of D61 and Y62 in the D′E-loop. The loss of the phenol also eliminates its van der Waals and polar interactions with K364 and K366, shifting the terminal amino group of K364 away from the D′E-loop, which sequentially displaces the guanidinium of R362 and the imidazole ring of H426 from the D′E-loop. The end result for Y279C is weakened van der Waals and polar interactions between the D′E-loop in the N-SH2 domain and the pY-loop, WPD-loop, and E-loop in the PTP domain. The A461T mutation (Figure 2B) introduces steric repulsion with Y62 in the D′E-loop and Y279 in the pY-loop and pushes both residues away from the active site. Displacement of Y279 triggers repositioning of the R278 side chain, disrupting the R278-bridged H-bond network (i.e., R278 with the side chain of S365 and backbone oxygens of K366, G332, and C333) that functions to restrain the E-loop for a well-defined active pocket in wild-type SHP2. As a result, the E-loop in A461T moves away from the active site, losing its interaction with the D′E-loop in the N-SH2 domain. The G464A mutation (Figure 2C) creates a strong steric clash with the backbone oxygen of G60, which triggers local conformational changes in G60 and the adjacent T59. These conformational changes drive the D′E-loop ~1 Å from the active site and weaken van der Waals and polar interactions between T59 and R362, abolishing the interaction of the E-loop with the D′E-loop. The T468M mutation (Figure 2D) causes steric repulsion with W423 in the WPD-loop, pushing the WPD-loop and nearby E-loop slightly away from the D′E-loop and therefore weakening the N-SH2−PTP interdomain interaction. In the Q506P mutant (Figure 2E), the loss of the glutamine side chain weakens van der Waals interaction with nearby D′E-loop residues. More importantly, the Q506P mutation eliminates two interdomain H-bonds formed by Q506 with the side chain of N58 and main chain of A72, thus weakening the N-SH2−PTP interdomain interaction. The Q510E mutation (Figure 2F) does not induce any noticeable structural changes, but unlike the amide group in glutamine, the carboxylate side chain in a glutamic acid cannot form a hydrogen bond with the backbone oxygen of G60 in the D′E-loop, leading to a weakening of the N-SH2−PTP interdomain interaction. Collectively, these structural observations provide direct evidence that the N-SH2−PTP interdomain interaction is destabilized in LS-associated SHP2 mutants. Consequently, LS SHP2 mutants may have an inherently stronger tendency, compared to that of the wild-type enzyme, to undergo the transition from a closed, autoinhibited conformation to an open, activated state.

Molecular Basis for the Catalytic Impairment of the LS-Associated SHP2 Mutants. In addition to revealing an

dx.doi.org/10.1021/bi5002695 | *Biochemistry* 2014, 53, 4136−4151

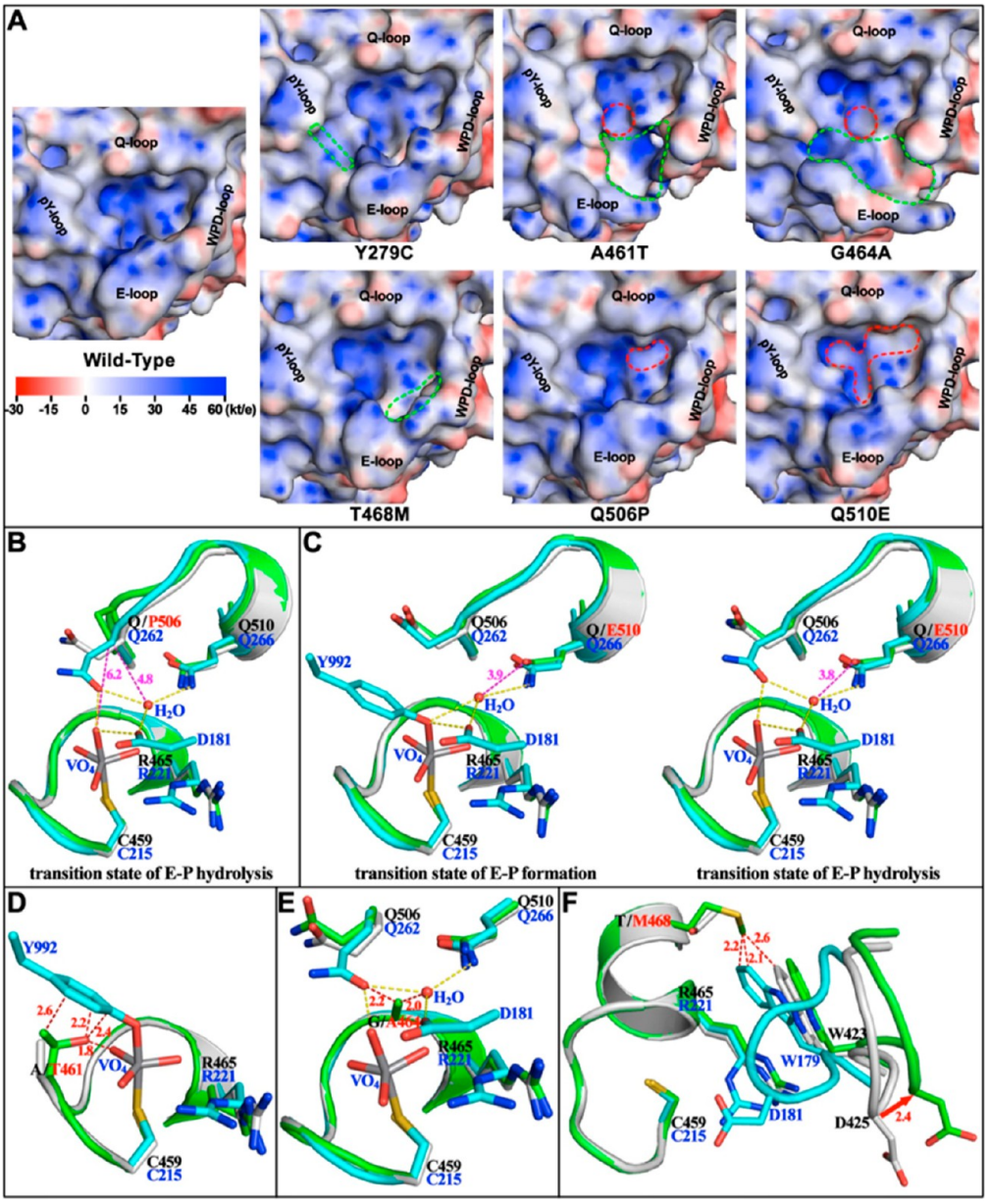

Figure 3. Structural basis for the impaired phosphatase activity associated with LS SHP2 mutants. (A) Active site pocket of wild-type SHP2 and six LS mutants. The surface is colored by electrostatic potential. The altered surfaces in the LS mutant are highlighted with a green dashed line, and areas with decreased positive electrostatic potential are highlighted with red dashed lines. (B) The Q506P mutation abolishes the ability to coordinate the attacking nucleophilic water in the E-P hydrolysis step. The complex structures of PTP1B·VO_4 (PDB entry 3I8O, cyan, which mimics the transition state of E-P hydrolysis) and the SHP2 Q506P mutant (PDB entry 4OHH, green) were superimposed onto that of wild-type SHP2 (PDB entry 4DGP, gray) to illustrate the abrogated hydrogen bonds (indicated by purple dashed lines with distances labeled). The black (or red for highlighting the LS mutation) residue labels are for SHP2 and the blue labels for PTP1B. The yellow dashed lines represent the well-defined H-bond network in the transition state. The representation scheme in panel B is also applied to panels C–F. (C) The Q510E mutation abrogates an H-bond with structurally conserved water and destabilizes the transition state of E-P formation and E-P hydrolysis. The complex structure of PTP1B·EGFR(Y992)-peptide·VO_4 (PDB entry 3I7Z, cyan, which mimics the transition state of E-P formation) or PTP1B·VO_4 (PDB entry 3I8O, cyan) and that of the SHP2 Q510E mutant (PDB entry 4OHI, green) were superimposed onto that of wild-type SHP2 (PDB entry 4DGP, gray) to illustrate the abrogated hydrogen bonds (indicated by purple dashed lines with distances labeled). (D) The A461T mutation introduces strong steric repulsions with the bound pTyr and destabilizes the transition state of E-P formation. The complex structures of PTP1B·EGFR(Y992)-peptide·VO_4 (PDB entry 3I7Z, cyan) and the SHP2 A461T mutant (PDB entry 4OHD, green) were superimposed onto that of wild-type SHP2 (PDB entry 4DGP, gray) to illustrate the steric repulsions (highlighted by red dashed lines with distances labeled). (E) The G464A mutation introduces strong steric repulsion with Q506 and structurally conserved water in the transition state of E-P hydrolysis. The complex structures of PTP1B·VO_4 (PDB entry 3I8O, cyan) and the SHP2 G464A mutant (PDB entry 4OHE, green) were superimposed onto that of wild-type SHP2 (PDB entry 4DGP, gray) to illustrate the steric repulsion (highlighted by red dashed lines with distances labeled). (F) The T468M mutation introduces strong steric repulsion with W423 within the closed WPD-loop. The complex structures of PTP1B·EGFR(Y992)-peptide·VO_4 (PDB entry 3I7Z, cyan) and the SHP2 T468M mutant (PDB entry 4OHL, green) were superimposed onto that of wild-type SHP2 (PDB entry 4DGP, gray) to illustrate the steric repulsion (highlighted by red dashed lines with distances labeled).

dx.doi.org/10.1021/bi5002695 | *Biochemistry* 2014, 53, 4136–4151

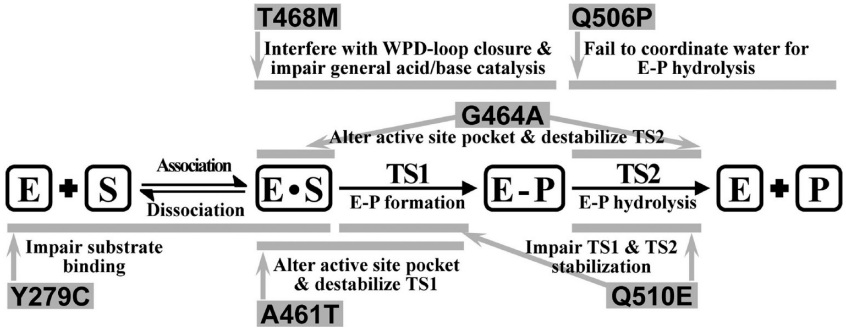

Figure 4. Schematic diagram showing the impact of LS-associated SHP2 mutations on the SHP2-catalyzed reaction.

altered "molecular switch" mechanism for the LS-associated SHP2 mutants, the availability of the mutant structures also provides an opportunity to examine the molecular basis for the impaired phosphatase activity associated with the LS SHP2 mutants. The PTP-catalyzed reaction proceeds via a two-step mechanism involving a covalent intermediate.[46] Following substrate binding, nucleophilic attack by the active site cysteine (C459 in SHP2) occurs on the substrate phosphorus atom in the first catalytic step, leading to the formation of a thiophosphoryl enzyme intermediate (E-P).[47,48] E-P formation is assisted by a conserved aspartic acid (D425 in SHP2) in the WPD-loop, functioning as a general acid, to neutralize the buildup of a negative charge on the leaving group.[49,50] In the second catalytic step, E-P hydrolysis by a water molecule is assisted by D425, which functions as a general base, with subsequent release of the free enzyme and inorganic phosphate.[51,52] In addition, the two conserved glutamine residues (Q506 and Q510 in SHP2) in the Q-loop are important for the precise placement of the water nucleophile for efficient E-P hydrolysis.[53,54] The PTPs further accelerate E-P formation and hydrolysis by preferentially binding the pentacoordinated transition states with the guanidinium side chain of the active site arginine (R465 in SHP2) and the main chain amides of the P-loop residues (C^{459}SAGIGR^{465}).[55−58]

Y279 in the pY-loop is involved in $\pi-\pi$ stacking interaction with the benzene ring of pTyr and sets the depth of the PTP active site pocket.[59] Our previous Y279C structure shows how this mutation alters the molecular surface of the active site, thereby weakening substrate binding and impairing catalysis.[36] Similarly, the current crystal structures also uncover the molecular basis of the impaired activity for other LS SHP2 mutants. Q506 and Q510 are invariant among the PTPs and are located in a surface loop (Q-loop) near the active site. Q506P and Q510E mutations do not alter the shape of the active site pocket but appear to decrease the positive electrostatic potential within the active site (Figure 3A). Previous structural and mutagenesis analyses of the cognate glutamine residues in *Yersinia* PTP and PTP1B have shown that Q506 is important for the optimal positioning of the nucleophilic water in the hydrolysis of the E-P intermediate, while Q510 plays an important role for both E-P formation and breakdown through a water-mediated hydrogen bonding network with the phosphoryl moiety.[53,54,60] Indeed, structural superimposition of PTP1B·VO_4 (PDB entry 3I8O),[60] which mimics the transition state for E-P hydrolysis, and SHP2/Q506P onto the wide-type SHP2 structure revealed that the Q506P mutation disrupts the hydrogen bond between the side chain of Q506 and the apical oxygen in vanadate, which is equivalent to the oxygen atom of the attacking nucleophilic water in the E-P hydrolysis step (Figure 3B). Similar structural comparison of PTP1B·EGFR/pY992-peptide·VO_4 (PDB entry 3I7Z),[60] which mimics the transition state of E-P formation, or PTP1B·VO_4 with SHP2/Q510E showed that the Q510E mutation abrogates a hydrogen bond with a conserved structural water, which interacts with the apical oxygen and one of the equatorial oxygens in the oxyanion (Figure 3C). Thus, the Q510E mutant destabilizes the transition states for both of the chemical steps.

A461 and G464 reside within the "signature motif" **C**XAGXG**R** that defines the PTP family and comprises the P-loop in PTP structures. As shown in Figure 3A, the active site pocket in A461T or G464A is significantly altered, being much broader and less electropositive especially around the catalytic C459 because of the displacement of the E-loop. Thus, A461T or G464A may not be able to bind and precisely position pTyr for efficient catalysis. To improve our understanding of the impact of these P-loop mutations on SHP2 catalysis, we superimposed the structures of PTP1B·EGFR/pY992-peptide·VO_4 and SHP2/A461T onto the SHP2 wild-type structure. As shown in Figure 3D, substitution of A461 with a Thr imposes a strong steric clash (highlighted by red dashed lines with distances labeled in red) with the bound pTyr and destabilizes the transition state for E-P formation, therefore impairing the activity of the A461T mutant. Superimposition of the structures of PTP1B·VO_4 and SHP2/G464A onto the SHP2 wild-type structure revealed why G464A has a lower phosphatase activity. Unlike the situation in the wild-type SHP2 structure, Q506 (Q262 in PTP1B) in SHP2/G464A is unable to make the necessary conformational change to be in position to coordinate water-mediated E-P hydrolysis (Figure 3E), because of an unfavorable obstruction by the substituted Ala at residue 464. As shown in Figure 3A, the T468M mutation introduces steric repulsion with W423, which drives the WPD-loop ∼2 Å from active site and creates a slightly broader active site pocket. More importantly, structural superimposition of PTP1B·EGFR/pY992-peptide·VO_4 and SHP2/T468M onto the wild-type SHP2 structure showed that substitution of T468 with Met leads to strong steric hindrance with W423 (W179 in PTP1B) within the closed WPD-loop, which would prevent WPD-loop closure and efficient general acid/base catalysis by D425. Taken together, our structural analyses illuminate the molecular basis for the reduced catalytic activity that is characteristic of the LS-associated SHP2 mutants. Although further experimentation will be required to substantiate these conclusions, catalytic impairments induced by the LS mutations appear to range from weakened substrate binding to misalignment of active site residues and weakened transition-state stabilization (Figure 4).

dx.doi.org/10.1021/bi5002695 | *Biochemistry* 2014, 53, 4136−4151

The LS-Associated SHP2 Mutants Have an Increased Propensity To Adopt the Open Conformation. Our structural studies described above indicate that although LS-associated SHP2 mutants are in the closed conformation, the N-SH2−PTP interdomain interaction is significantly compromised in the mutants. To furnish additional evidence that this interdomain interaction is weakened in the LS SHP2 mutants, we measured the ability of the isolated N-SH2 domain to inhibit the phosphatase activity of the wild-type and LS SHP2 mutant catalytic domains. We previously established that the N-SH2 domain competitively inhibits SHP2 PTP domain-catalyzed *p*NPP hydrolysis.[36] The competitive nature is in line with the structural observation that the N-SH2 domain interacts with the PTP domain, thus blocking access of the substrate to the active site. Our prediction was that the dissociation constants (K_i values) for the N-SH2 domain and the LS SHP2 mutant PTP domain binary complexes would be larger than that for the binding of N-SH2 to the wild-type catalytic domain. As a control, the N-SH2 domain bearing the GOF E76K mutation displayed no inhibitory activity against the SHP2 PTP domain even at 200 μM N-SH2/E76K, which is consistent with the expectation that the full-length E76K mutant is in a constitutive active and open conformation. With the exception of A461T, which had an extremely low activity that prevented accurate measurement of the inhibition constant, the K_i values for the N-SH2 domain-mediated inhibition of LS SHP2 mutant PTP domains were determined and are summarized in Table 5. In support of the prediction from the steady-state kinetic data (Table 1) that R498L may already exist in the open conformation, the N-SH2 domain failed to inhibit the R498L PTP reaction at a concentration of 200 μM. Moreover, the results indicate the LS SHP2 mutant PTP domains were less inhibited by the N-SH2 domain as evidenced by the 1.5−98-fold increase in the K_i values compared to that of the wild-type enzyme (Table 5). Collectively, the inhibition data confirm the structural observations that revealed that the interdomain interaction between the N-SH2 and PTP domains is weakened in the LS-asociated SHP2 mutants.

Table 5. K_i Values for the Isolated N-SH2 Domain-Mediated Inhibition of the PTP Domain of Wild-Type SHP2 and Its LS Mutants

	K_i (μM)
WT	1.3 ± 0.1
Y279C	11.3 ± 0.3
A461T	not detectable
G464A	66.0 ± 5.8
T468M	2.0 ± 0.1
R498L	no inhibition at 200 μM
Q506P	41.9 ± 1.3
Q510E	128 ± 4

On the basis of the results from our structural and kinetic studies, it appears that, relative to wild-type SHP2, the LS SHP2 mutants have a stronger propensity to undergo the transition from a closed, autoinhibited conformation to an open, activated form. To gather more direct evidence of the increased "openness" for the LS mutants, we investigated the overall solution dynamic properties of wild-type SHP2, GOF mutant E76K, and all seven LS SHP2 mutants using hydrogen/deuterium exchange mass spectrometry (H/DX-MS). The H/DX-MS technique allows analysis of protein conformational dynamics in solution by measuring the exchange of backbone amide hydrogens with the deuterium bulk solvent.[61,62] We identified 38 peptides for each protein, covering 92% of the SHP2 sequence (residues 1−528). We determined backbone amide H/D exchange for each protein, calculated the differences in deuterium uptake between the mutant and wild-type SHP2 for each peptide at each time point, and generated both two-dimensional and three-dimensional "heat maps" showing the differential H/D exchange experienced by the mutants and the wild-type enzyme (Figure 5).

The GOF E76K mutant was used as a reference for H/D exchange magnitude and location experienced in a "true" SHP2 open conformation. Figure 5 shows that in comparison with wild-type SHP2, a number of peptides in E76K, located in the interface between the N-SH2 and PTP domains, display significant increases in their levels of deuterium incorporation. Within the N-SH2 domain, these peptides reside in the D′E-loop and adjacent β-strands B−D, D′, E, and F, structural elements known to participate in binding the PTP domain. Within the PTP domain, these peptides represent the catalytic loops at the active site, including the P-loop, pY-loop, E-loop, and Q-loop. Given the lack of inhibition of the PTP domain by N-SH2/E76K, the observed increase in the level of deuterium uptake surrounding the N-SH2 and PTP binding site suggests that the interdomain binding interface is solvent-exposed, providing direct evidence that E76K exists in an open and active conformation. Notably, LS mutant R498L exhibits an H/D exchange profile very similar to that of the E76K mutant (Figure 5), indicating that like E76K, R498L is also in the open conformation. H/D exchange data show that the six other LS-associated SHP2 mutants also experience increased deuterium uptake in the interface between the N-SH2 and PTP domains, albeit to a lesser degree in comparison with the peptides observed in E76K. The overall extents of H/D exchange decrease in the following order: R498L > Q510E ≈ Q506P > G464A > Y279C > A461T ≈ T468M [generally in accordance with the degree by which the catalytic domain is inhibited by the N-SH2 domain (Table 5), suggesting that the weakened N-SH2−PTP interaction in LS SHP2 mutants may be responsible for the increased dynamics in the N-SH2−PTP interdomain interface]. The increased deuterium uptake in the N-SH2−PTP interface in LS SHP2 mutants indicates that this interface is more dynamic and solvent-exposed, which supports the notion that LS SHP2 mutants may have an inherently stronger tendency, compared to the wild-type enzyme, to undergo the transition from a closed, autoinhibited conformation to an open, activated state.

LS-Associated SHP2 Mutations Engender GOF Phenotypes. Results from our kinetic, structural, and biophysical experiments suggest that LS mutations destabilize the closed SHP2 conformation and increase the propensity of the mutants to adopt the open conformation. It has been suggested that there is negative cooperativity between N-SH2 domain's intramolecular binding with the PTP domain and its intermolecular association with a pTyr-containing scaffolding protein.[14] Thus, engagement of the N-SH2 domain to a specific pTyr peptide will weaken its autoinhibitory interaction with the PTP domain, whereas a weakened intramolecular N-SH2−PTP interaction may enhance binding of N-SH2 with its pTyr-containing partners. Given the observed decrease in the strength of the N-SH2−PTP interaction, LS SHP2 mutants are expected to show increased affinity for adapter proteins. A

dx.doi.org/10.1021/bi5002695 | *Biochemistry* 2014, 53, 4136−4151

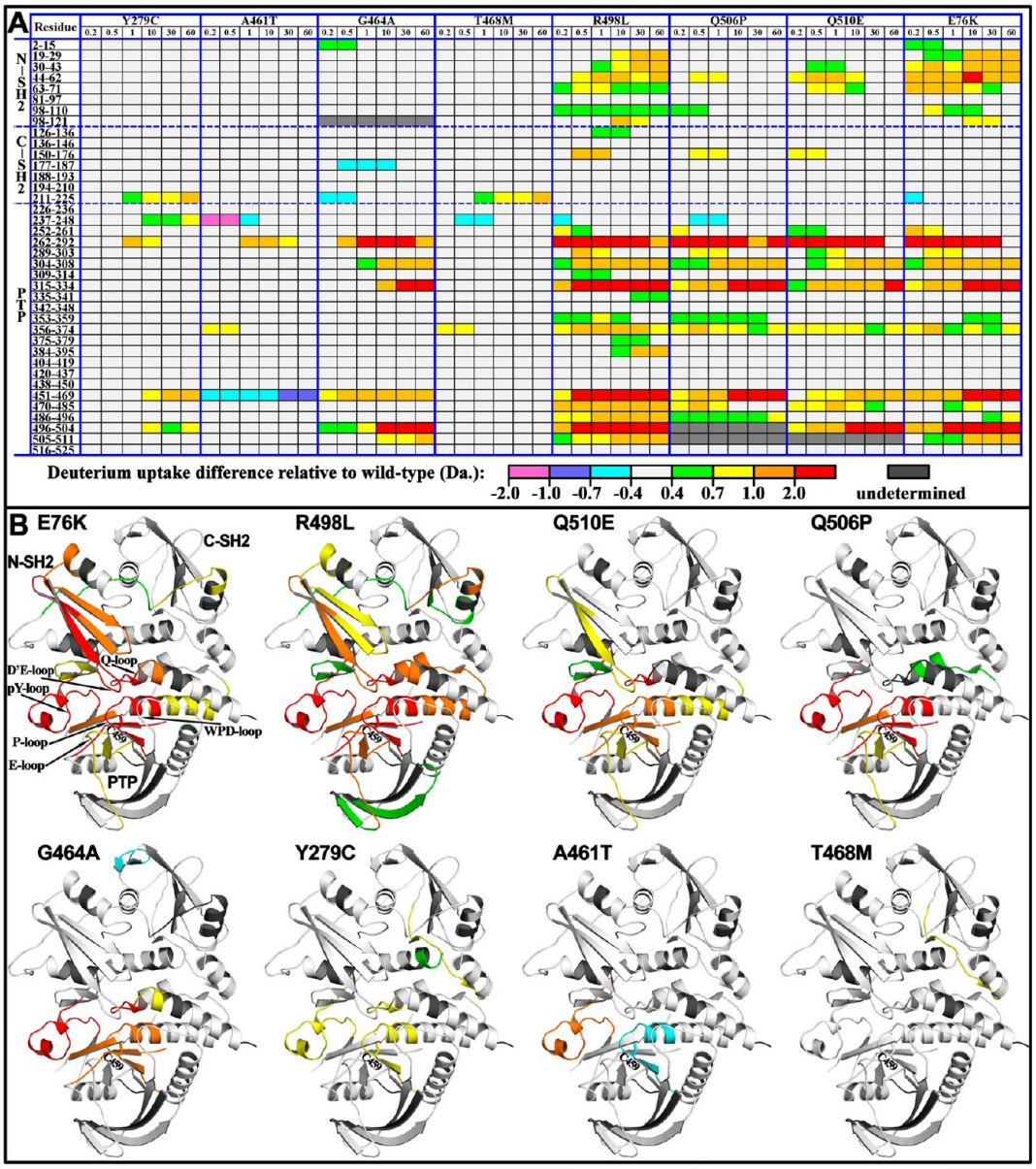

Figure 5. LS SHP2 mutants have conformational dynamics and propensities for the open conformation higher than those of the wild type. (A) Two-dimensional conformational dynamics heat map, characterized by differences in deuterium uptake between mutant and wild-type SHP2 on 38 peptides at various time points (0.2, 0.5, 1, 10, 30, and 60 min). (B) Differential hydrogen/deuterium exchange experienced by the LS and E76K SHP2 mutants, relative to the wild-type enzyme. Differential exchange data at the 10 min time point are mapped on the wild-type SHP2 crystal structure (PDB entry 4DGP). Peptides in SHP2 mutants are color-coded on the basis of an increased or decreased level of exchange relative to that of the wild type as described for panel A.

major SHP2 binding partner is Grb2-associated binder-1 (Gab1),[63] which becomes tyrosine-phosphorylated upon growth factor stimulation. Through its N-SH2 domain binding to the pTyr sequence motif in Gab1, SHP2 is directed to its physiological substrate(s) to drive RAS-ERK1/2 pathway activation.[64,65] To demonstrate that the LS SHP2 mutants indeed display enhanced binding affinity for Gab1, we investigated the effects of wild-type SHP2, GOF E76K, and all seven LS SHP2 mutants on epidermal growth factor (EGF) signaling in human embryonic kidney 293 (HEK293) cells as previously described.[35,36,66] Consistent with the prediction that the N-SH2 domain of LS SHP2 mutants has a higher affinity for pTyr ligands, the LS SHP2 mutants as well as the GOF E76K mutant, which is known to favor the open conformation, more readily formed complexes with Gab1 upon EGF stimulation (Figure 6A). Overall, the relative affinity for Gab1 displayed by the LS SHP2 mutants tracks well with the extent of H/D exchange experienced in the N-SH2−PTP interface (Figure 5), which is a measure of the openness for SHP2. Importantly, the enhanced Gab1 binding exhibited by the LS SHP2 mutants persisted up to 60 min after EGF stimulation, when no association was notable between wild-type SHP2 and Gab1. Thus, the LS SHP2 mutants can preferentially bind the upstream adaptor Gab1 (compared to wild-type SHP2) and stay longer on the scaffolding protein. We speculated that the increased residence time on Gab1 could prolong substrate turnover by the LS SHP2 mutants, which could compensate for their reduced phosphatase activity. To this end, we assessed the ability of wild-type and mutant SHP2 enzymes to dephosphorylate Paxillin/pY118, a physiological substrate of SHP2

dx.doi.org/10.1021/bi5002695 | *Biochemistry* 2014, 53, 4136−4151

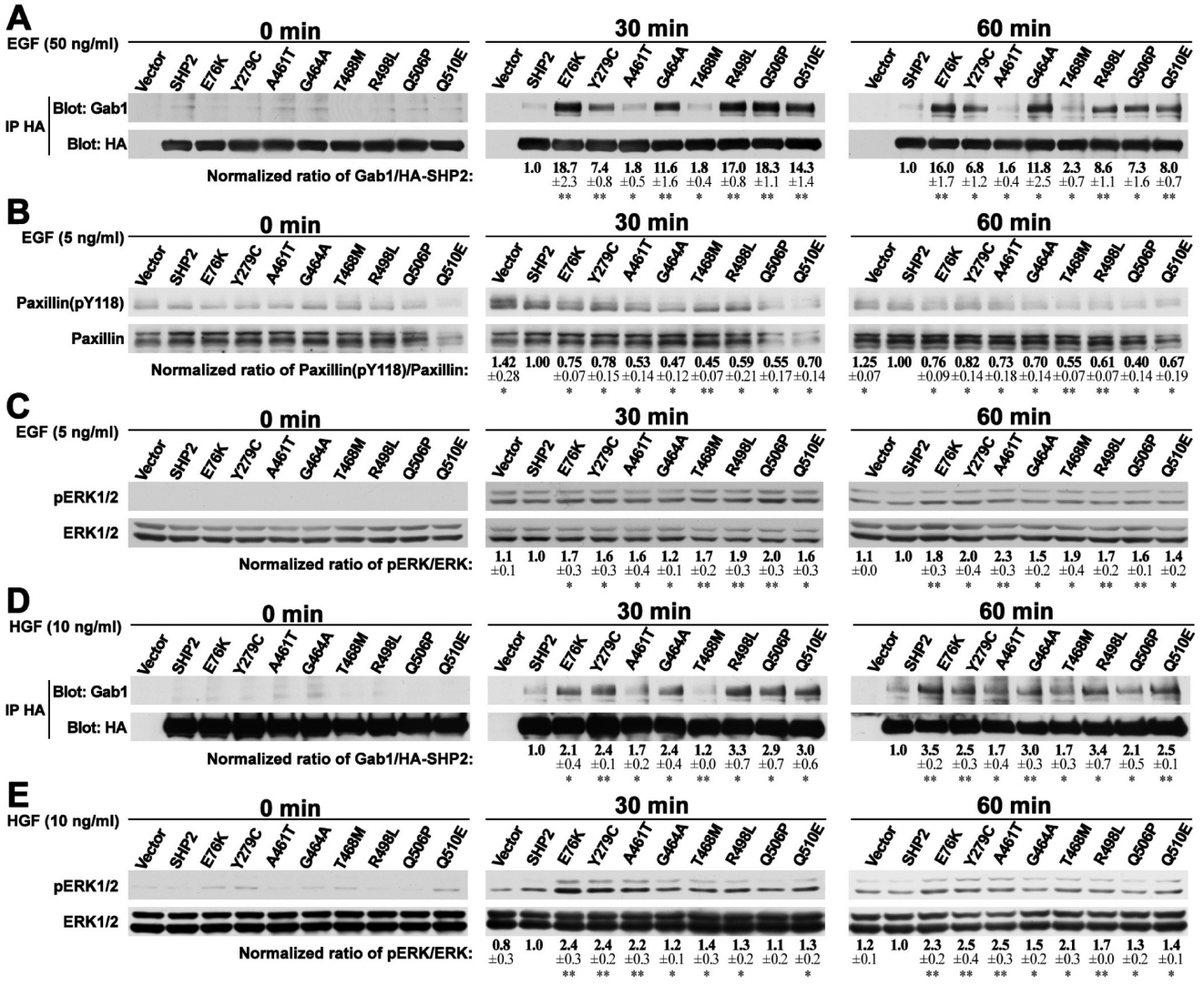

Figure 6. LS SHP2 mutations engender GOF effects on the RAS-ERK1/2 signaling pathway. (A) LS SHP2 mutants preferentially associate with and stay longer with Gab1 under EGF stimulation. (B) LS SHP2 mutants dephosphorylate the physiological substrate paxillin more efficiently. (C) LS SHP2 mutations enhance EGF-induced ERK1/2 activation. (D) LS SHP2 mutants preferentially associate with and stay longer with Gab1 under HGF stimulation. (E) LS SHP2 mutations enhance HGF-induced ERK1/2 activation. All results shown in this figure were representative of two to four independent experiments; the numbers below each panel are means ± the standard deviation, and the statistical significance is indicated (*P < 0.05; **P < 0.01). Quantification and normalization were performed as follows. Band intensity was quantified using ImageJ, and the Gab1/HA-SHP2 (for panels A and D), pPaxillin(pY118)/total Paxillin (for panel B), and pERK1/2/total ERK1/2 (for panels C and E) ratios were normalized to the ratio in wild-type SHP2-overexpressing cells.

required for EGF-stimulated ERK1/2 activation.[44] Figure 6B shows that, like the GOF E76K mutant, the LS SHP2 mutants were more efficient in dephosphorylating Paxillin/pY118.

SHP2/Gab1 binding and SHP2-mediated dephosphorylation of Paxillin/pY118 are two recognized signaling events shown to be important for EGF-induced ERK1/2 phosphorylation.[44,64] Given the higher affinity for Gab1 and increased level of Paxillin/pY118 dephosphorylation by the LS SHP2 mutants, LS SHP2 mutations are expected to engender a GOF effect on ERK1/2 activation. To determine whether LS SHP2 mutants are capable of activating the ERK1/2 pathway, we measured EGF-induced ERK1/2 phosphorylation in HEK293 cells overexpressing wild-type and mutant SHP2 (Figure 6C). Compared to that of wild-type SHP2-expressing cells, the level of ERK1/2 phosphorylation was further elevated and sustained in cells expressing the GOF E76K mutant as well as the LS SHP2 mutants. To make sure that the observed GOF effects exhibited by the LS mutants were not unique to EGF signaling, we also examined hepatocyte growth factor (HGF)-induced SHP2−Gab1 binding and subsequent ERK1/2 activation in cells overexpressing wild-type and mutant SHP2. Similar to EGF signaling, the SHP2−Gab1 interaction is also essential for HGF-mediated ERK1/2 activation downstream of the Met receptor.[67,68] Not surprisingly, the GOF E76K mutant and all LS SHP2 mutants exhibit enhanced Gab1 binding (Figure 6D) and ERK1/2 activation in HEK293 cells, especially at the later time point of 60 min following HGF stimulation (Figure 6E). Finally, to address the issue of whether the residual phosphatase activity associated with the LS SHP2 mutants is required for the GOF phenotype, we generated a double mutant in which the phosphatase activity of the Y279C mutant is eliminated by replacing the catalytic Cys459 with Ser and examined its effect on Gab1 binding and ERK1/2 activation upon either EGF or HGF stimulation. As shown in

dx.doi.org/10.1021/bi5002695 | Biochemistry 2014, 53, 4136−4151

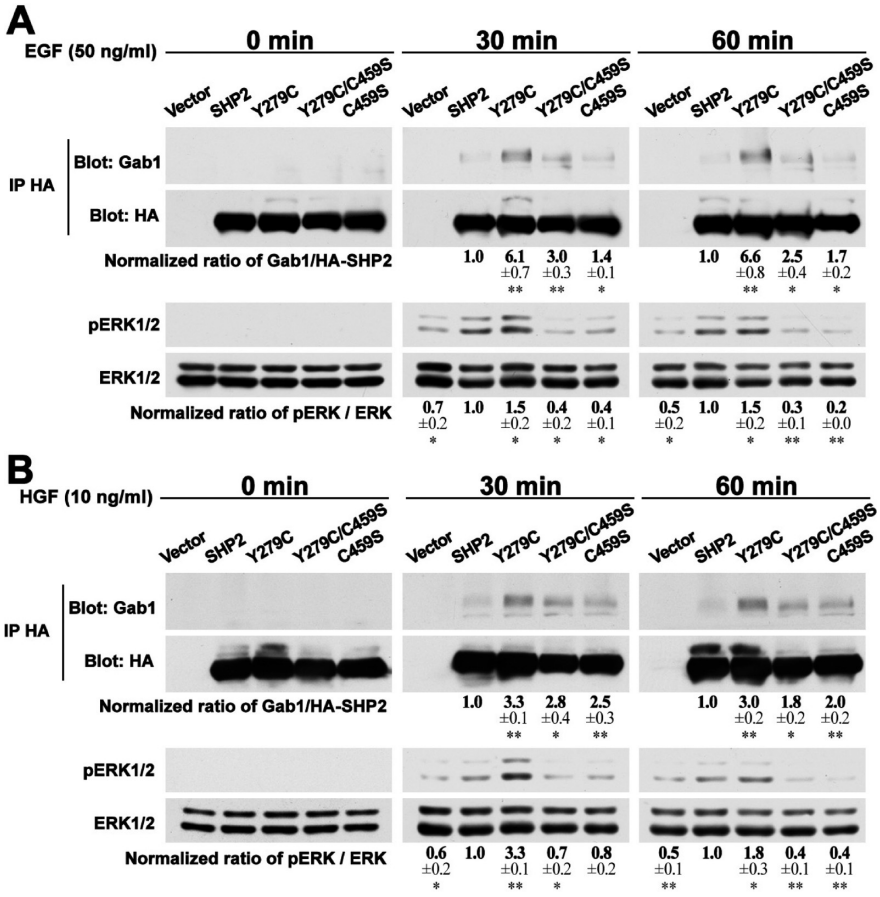

Figure 7. Residual phosphatase activity of LS SHP2 mutants is required for ERK1/2 activation. The catalytically dead Y279C/C459S double mutant was unable to activate ERK1/2 activation upon either EGF (A) or HGF (B) stimulation. The results shown in this figure are representative of two independent experiments; the numbers below each panel are means ± the standard deviation, and the statistical significance is indicated (*$P < 0.05$; **$P < 0.01$). Quantification and normalization processes are the same as those described in the legend of Figure 6.

Figure 7, although the catalytically dead double mutant Y279C/C459S still showed preferred and sustained binding with Gab1, it was unable to activate ERK1/2, indicating that the residual phosphatase activity associated with the LS SHP2 mutant is required for enhanced ERK1/2 activation. As a control, the C459S mutant was also unable to support growth factor-stimulated ERK1/2 activation. Collectively, the results show that LS SHP2 mutations engender GOF phenotypes and enhanced signaling through the ERK1/2 pathway is a general feature for all LS SHP2 mutants.

DISCUSSION

SHP2 is an allosteric enzyme regulated by an intramolecular switch between its N-SH2 and PTP domains. Unlike most other PTPs that terminate the action of PTKs, SHP2 promotes growth factor-mediated RAS-ERK1/2 activation.[6−8] Germline mutations in SHP2 are known to cause 90 and 50% of LS and NS cases, respectively,[69] two of several autosomal-dominant conditions collectively classified as "RASopathies", which are characterized by GOF mutations in components of the RAS-ERK1/2 pathway.[70] NS-associated SHP2 mutations cluster within the interface between the N-SH2 and PTP domains, which confer GOF properties to SHP2, presumably by alleviating the autoinhibitory effect of the N-SH2 domain upon the PTP active site.[28,30−33] Thus, NS-associated SHP2 mutants display increased phosphatase activity and promote sustained activation of the RAS-ERK1/2 pathway.[29,30,71] Similarly, GOF mutations in other components of the RAS-ERK1/2 pathway, such as RAS, RAF, and SOS1, have been identified in NS patients lacking SHP2 mutations.[72−79] Moreover, GOF mutations in RAS, RAF, or MEK1/2 also cause phenotypically overlapping Costelo and Cardiofaciocutaneous syndromes.[80−82] These observations underscore the fact that aberrant activation of the RAS-ERK1/2 pathway plays a key role in developing RASopathies.[83]

In contrast to NS-associated SHP2 mutations, LS-associated SHP2 mutations alter seven residues in the active site of the PTP domain, yielding mutant enzymes with reduced phosphatase activity.[24,25,32,34−36] Because of the impaired catalytic activity, LS-associated SHP2 mutants were initially suggested to be LOF variants.[35] However, from a genetic perspective, it is worth noting that the LS-associated SHP2 alleles are specific missense mutations. If their sole effect in transducing their phenotype was to reduce or eliminate SHP2's phosphatase activity, the existence of some haploinsufficient alleles such as nonsense mutations might be anticipated, but none has been observed.[24,25] One report suggested that LS-associated SHP2 mutants can act as dominant negatives that inhibit growth factor-evoked ERK1/2 activation in transfection assays.[35] Zebrafish embryos injected with mRNA encoding LS SHP2 mutations do not show ERK1/2 activation in neural crest,[84] and the Y279C knock-in mouse model shows Akt hyperactivation, but not ERK1/2 hyperactivation, in the heart.[85] Other studies reveal that ubiquitous expression of

dx.doi.org/10.1021/bi5002695 | *Biochemistry* 2014, 53, 4136−4151

two of the most recurrent LS-causing SHP2 alleles (Y279C and T468M) in *Drosophila* leads to GOF phenotypes that lead to heightened EGF-mediated RAS-ERK1/2 pathway activation,[86] which were similar to those observed with NS-causing SHP2 mutant transgenic flies.[31] Importantly, experiments with the Y279C/R465M transgenic fly suggest that the LS SHP2 mutant's residual phosphatase activity was required for the GOF developmental effects.[86] Our data with a catalytically dead double mutant Y279C/C459S provide further evidence that the residual phosphatase activity associated with the LS SHP2 mutant is required for enhanced ERK1/2 activation (Figure 7). Consistent with findings in the *Drosophila* LS model, MEK1 and basal ERK1/2 phosphorylation levels were elevated in induced pluripotent stem cells from LS patients.[87] Importantly, GOF mutations in RAF1[76] and BRAF[78] are also found in LS patients, indicating that like all RASopathies, enhanced RAS-ERK1/2 signaling is responsible for the pathogenesis of LS, as well.

How do catalytically impaired LS-associated SHP2 mutants engender GOF phenotypes? To begin to answer this question, we took a multidisciplinary approach, involving a combination of enzyme kinetics, site-directed mutagenesis, X-ray crystallography, H/D exchange mass spectrometry, and cell biology to characterize the structural and biochemical properties of LS-associated SHP2 mutants encompassing all seven known LS SHP2 mutation sites. Rigorous kinetic analyses with both *p*NPP- and pTyr-containing peptide substrates indicate that LS SHP2 mutations lead to significantly reduced SHP2 phosphatase activity. Detailed comparison of the mutant crystal structures with those of wild-type SHP2 and PTP1B in complex with a substrate and/or a transition-state mimetic reveals that the observed catalytic impairments in the LS-associated SHP2 mutants are caused by a number of mechanisms, including weakened substrate binding, perturbation of active site residue alignment, and weakened transition-state stabilization. Importantly, we found that although the LS-associated SHP2 mutants still exist in the closed autoinhibited conformation, the intramolecular N-SH2−PTP interdomain interaction in the mutants is significantly weakened, leading to mutant enzymes with an inherently higher propensity, compared to that of the wild-type enzyme, to be activated by engagement of its N-SH2 domain with pTyr motifs in growth factor receptors and scaffolding proteins and to adopt an open, activated state. As a consequence, LS-associated SHP2 mutants bind upstream activators (e.g., Gab1) preferentially and stay longer with scaffolding adapters, thus prolonging specific substrate turnover (e.g., Paxillin), which compensates for the reduced phosphatase activity and engenders GOF phenotypes through sustained activation of the RAS-ERK1/2 pathway. It should also be noted that SHP2 is known to be tyrosine-phosphorylated on two C-terminal Tyr residues (Tyr542 and Tyr580), which can apparently activate SHP2 by intramolecular SH2 binding.[88−90] It is thus possible that an increased level of interaction between the N-SH2 domain and the C-terminal tyrosine phosphorylation sites may also contribute to LS SHP2 mutant-mediated hyper-ERK1/2 activation. Overall, this study provides new insight into the molecular basis of LS-associated SHP2 mutations as well as the biochemical mechanism that underlies the pathological processes mediated by the LS SHP2 mutants. Our results also serve as a useful framework for studying other disease-associated SHP2 mutations that may have an impact on future drug development targeting SHP2.

■ ASSOCIATED CONTENT

Accession Codes

Coordinates and structure factors for LS SHP2 mutants have been deposited in Protein Data Bank as entries 4OHD for A461T, 4OHE for G464A, 4OHL for T468M, 4OHH for Q506P, and 4OHI for Q510E.

■ AUTHOR INFORMATION

Corresponding Author

*E-mail: zyzhang@iu.edu.

Author Contributions

Z.-H.Y. and R.-Y.Z. contributed equally to this work.

Funding

This work was supported by National Institutes of Health Grant RO1 CA69202.

Notes

The authors declare no competing financial interest.

■ ABBREVIATIONS

EGF, epidermal growth factor; ERK, extracellular signal-regulated kinase; Gab1, Grb2-associated binder-1; GOF, gain-of-function; H/DX-MS, hydrogen/deuterium exchange mass spectrometry; HGF, hepatocyte growth factor; LOF, loss-of-function; LS, LEOPARD syndrome; NS, Noonan syndrome; *p*NPP, *p*-nitrophenyl phosphate; PTK, protein tyrosine kinase; PTP, protein tyrosine phosphatase; pTyr, phosphotyrosine; rmsd, root-mean-square deviation; SH2, Src homology 2.

■ REFERENCES

(1) Hunter, T. (2009) Tyrosine phosphorylation: Thirty years and counting. *Curr. Opin. Cell Biol. 21*, 140−146.

(2) Tonks, N. K. (2006) Protein tyrosine phosphatases: From genes, to function, to disease. *Nat. Rev. Mol. Cell Biol. 7*, 833−846.

(3) Zhang, Z.-Y. (2001) Protein tyrosine phosphatases: Prospects for therapeutics. *Curr. Opin. Chem. Biol. 5*, 416−423.

(4) Arena, S., Benvenuti, S., and Bardelli, A. (2005) Genetic analysis of the *kinome* and *phosphatome* in cancer. *Cell. Mol. Life Sci. 62*, 2092−2099.

(5) Ventura, J. J., and Nebreda, A. R. (2006) Protein kinases and phosphatases as therapeutic targets in cancer. *Clin. Transl. Oncol. 8*, 153−160.

(6) Neel, B. G., Gu, H. H., and Pao, L. (2003) The 'Shp'ing news: SH2 domain-containing tyrosine phosphatases in cell signaling. *Trends Biochem. Sci. 28*, 284−293.

(7) Chan, R. J., and Feng, G. S. (2007) PTPN11 is the first identified proto-oncogene that encodes a tyrosine phosphatase. *Blood 109*, 862−867.

(8) Grossmann, K. S., Rosário, M., Birchmeier, C., and Birchmeier, W. (2010) The tyrosine phosphatase Shp2 in development and cancer. *Adv. Cancer Res. 106*, 53−89.

(9) Perkins, L. A., Larsen, I., and Perrimon, N. (1992) *Corkscrew* encodes a putative protein tyrosine phosphatase that functions to transduce the terminal signal from the receptor tyrosine kinase torso. *Cell 70*, 225−236.

(10) Noguchi, T., Matozaki, T., Horita, K., Fujioka, Y., and Kasuga, M. (1994) Role of SH-PTP2, a protein-tyrosine phosphatase with src homology 2 domains, in insulin-stimulated Ras activation. *Mol. Cell. Biol. 14*, 6674−6682.

(11) Herbst, R., Carroll, P. M., Allard, J. D., Schilling, J., Raabe, T., and Simon, M. A. (1996) Daughter of sevenless is a substrate of the phosphotyrosine phosphatase Corkscrew and functions during sevenless signaling. *Cell 85*, 899−909.

(12) Gutch, M. J., Flint, A. J., Keller, J., Tonks, N. K., and Hengartner, M. O. (1998) The *Caenorhabditis elegans* SH2 domain-containing

protein tyrosine phosphatase PTP2 participates in signal transduction during oogenesis and vulval development. *Genes Dev. 12*, 571−585.
(13) Dance, M., Montagner, A., Salles, J. P., Yart, A., and Raynal, P. (2008) The molecular functions of Shp2 in the Ras/mitogen-activated protein kinase (ERK1/2) pathway. *Cell. Signalling 20*, 453−459.
(14) Hof, P., Pluskey, S., Dhe-Paganon, S., Eck, M. J., and Shoelson, S. E. (1998) Crystal structure of the tyrosine phosphatase SHP2. *Cell 92*, 441−450.
(15) Barford, D., and Neel, B. G. (1998) Revealing mechanisms for SH2 domain mediated regulation of the protein tyrosine phosphatase SHP-2. *Structure 6*, 249−254.
(16) Pei, D., Wang, J., and Walsh, C. T. (1996) Differential functions of the two Src homology 2 domains in protein tyrosine phosphatase SHPTP1. *Proc. Natl. Acad. Sci. U.S.A. 93*, 1141−1145.
(17) Pluskey, S., Wandless, T. J., Walsh, C. T., and Shoelson, S. E. (1995) Potent stimulation of SH-PTPs phosphatase activity by simultaneous occupancy of both SH2 domains. *J. Biol. Chem. 270*, 2897−2900.
(18) Sugimoto, S., Wandless, T. J., Shoelson, S. E., Neel, B. G., and Walsh, C. T. (1994) Activation of the SH2-containing protein tyrosine phosphatase, SH-PTP2, by phosphotyrosine-containing peptides derived from insulin receptor substrate-1. *J. Biol. Chem. 269*, 13614−13622.
(19) Loh, M. L., Vattikuti, S., Schubbert, S., Reynolds, M. G., Carlson, E., Lieuw, K. H., Cheng, J. W., Lee, C. M., Stokoe, D., Bonifas, J. M., Curtiss, N. P., Gotlib, J., Meshinchi, S., Le Beau, M. M., Emanuel, P. D., and Shannon, K. M. (2004) Mutations in PTPN11 implicate the SHP-2 phosphatase in leukemogenesis. *Blood 103*, 2325−2331.
(20) Tartaglia, M., Niemeyer, C. M., Fragale, A., Song, X. L., Buechner, J., Jung, A., Hahlen, K., Hasle, H., Licht, J. D., and Gelb, B. D. (2003) Somatic mutations in PTPN11 in juvenile myelomonocytic leukemia, myelodysplastic syndromes and acute myeloid leukemia. *Nat. Genet. 34*, 148−150.
(21) Bentires-Alj, M., Paez, J. G., David, F. S., Keilhack, H., Halmos, B., Naoki, K., Maris, J. M., Richardson, A., Bardelli, A., Sugarbaker, D. J., Richards, W. G., Du, J. Y., Girard, L., Minna, J. D., Loh, M. L., Fisher, D. E., Velculescu, V. E., Vogelstein, B., Meyerson, M., Sellers, W. R., and Neel, B. G. (2004) Activating mutations of the Noonan syndrome-associated SHP2/PTPN11 gene in human solid tumors and adult acute myelogenous leukemia. *Cancer Res. 64*, 8816−8820.
(22) Chan, G., Kalaitzidis, D., and Neel, B. G. (2008) The tyrosine phosphatase Shp2 (PTPN11) in cancer. *Cancer Metastasis Rev. 27*, 179−192.
(23) Miyamoto, D., Miyamoto, M., Takahashi, A., Yomogita, Y., Higashi, H., Kondo, S., and Hatakeyama, M. (2008) Isolation of a distinct class of gain-of-function SHP-2 mutants with oncogenic RAS-like transforming activity from solid tumors. *Oncogene 27*, 3508−3515.
(24) Digilio, M. C., Conti, E., Sarkozy, A., Mingarelli, R., Dottorini, T., Marino, B., Pizzuti, A., and Dallapiccola, B. (2002) Grouping of multiple-lentigines/LEOPARD and Noonan syndromes on the PTPN11 gene. *Am. J. Hum. Genet. 71*, 389−394.
(25) Legius, E., Schrander-Stumpel, C., Schollen, E., Pulles-Heintzberger, C., Gewillig, M., and Fryns, J. P. (2002) PTPN11 mutations in LEOPARD syndrome. *J. Med. Genet. 39*, 571−574.
(26) Tartaglia, M., and Gelb, B. D. (2005) Noonan syndrome and related disorders: Genetics and pathogenesis. *Annu. Rev. Genomics Hum. Genet. 6*, 45−68.
(27) Tartaglia, M., Mehler, E. L., Goldberg, R., Zampino, G., Brunner, H. G., Kremer, H., van der Burgt, I., Crosby, A. H., Ion, A., Jeffery, S., Kalidas, K., Patton, M. A., Kucherlapati, R. S., and Gelb, B. D. (2001) Mutations in PTPN11, encoding the protein tyrosine phosphatase SHP-2, cause Noonan syndrome. *Nat. Genet. 29*, 465−468.
(28) Keilhack, H., David, F. S., McGregor, M., Cantley, L. C., and Neel, B. G. (2005) Diverse biochemical properties of Shp2 mutants. Implications for disease phenotypes. *J. Biol. Chem. 280*, 30984−30993.
(29) Araki, T., Mohi, M. G., Ismat, F. A., Bronson, R. T., Williams, I. R., Kutok, J. L., Yang, W. T., Pao, L. I., Gilliland, D. G., Epstein, J. A., and Neel, B. G. (2004) Mouse model of Noonan syndrome reveals cell type- and gene dosage-dependent effects of Ptpn11 mutation. *Nat. Med. 10*, 849−857.
(30) Fragale, A., Tartaglia, M., Wu, J., and Gelb, B. D. (2004) Noonan syndrome-associated SHP2/PTPN11 mutants cause EGF-dependent prolonged GAB1 binding and sustained ERK2/MAPK1 activation. *Hum. Mutat. 23*, 267−277.
(31) Oishi, K., Gaengel, K., Krishnamoorthy, S., Kamiya, K., Kim, I. K., Ying, H. W., Weber, U., Perkins, L. A., Tartaglia, M., Mlodzik, M., Pick, L., and Gelb, B. D. (2006) Transgenic *Drosophila* models of Noonan syndrome causing PTPN11 gain-of-function mutations. *Hum. Mol. Genet. 15*, 543−553.
(32) Tartaglia, M., Martinelli, S., Stella, L., Bocchinfuso, G., Flex, E., Cordeddu, V., Zampino, G., van der Burgt, I., Palleschi, A., Petrucci, T. C., Sorcini, M., Schoch, C., Foa, R., Emanuel, P. D., and Gelb, B. D. (2006) Diversity and functional consequences of germline and somatic PTPN11 mutations in human disease. *Am. J. Hum. Genet. 78*, 279−290.
(33) Martinelli, S., Torreri, P., Tinti, M., Stella, L., Bocchinfuso, G., Flex, E., Grottesi, A., Ceccarini, M., Palleschi, A., Cesareni, G., Castagnoli, L., Petrucci, T. C., Gelb, B. D., and Tartaglia, M. (2008) Diverse driving forces underlie the invariant occurrence of the T42A, E139D, I282V and T468M SHP2 amino acid substitutions causing Noonan and LEOPARD syndromes. *Hum. Mol. Genet. 17*, 2018−2029.
(34) Hanna, N., Montagner, A., Lee, W. H., Miteva, M., Vidal, M., Vidaud, M., Parfait, B., and Raynal, P. (2006) Reduced phosphatase activity of SHP2 in LEOPARD syndrome: Consequences for P13K binding on Gab1. *FEBS Lett. 580*, 2477−2482.
(35) Kontaridis, M. I., Swanson, K. D., David, F. S., Barford, D., and Neel, B. G. (2006) PTPN11 (Shp2) mutations in LEOPARD syndrome have dominant negative, not activating, effects. *J. Biol. Chem. 281*, 6785−6792.
(36) Yu, Z. H., Xu, J., Walls, C. D., Chen, L., Zhang, S., Zhang, R. Y., Wu, L., Wang, L. N., Liu, S. J., and Zhang, Z.-Y. (2013) Structural and Mechanistic Insights into LEOPARD Syndrome-Associated SHP2Mutations. *J. Biol. Chem. 288*, 10472−10482.
(37) Zhang, Z.-Y., Thieme-Sefler, A. M., Maclean, D., Roeske, R., and Dixon, J. E. (1993) A Continuous Spectrophotometric and Fluorimetric Assay for Protein Tyrosine Phosphatase Using Phosphotyrosine Containing Peptides. *Anal. Biochem. 211*, 7−15.
(38) Otwinowski, Z., and Minor, W. (1997) Processing of X-ray diffraction data collected in oscillation mode. In *Macromolecular Crystallography, Part A*, pp 307−326, Academic Press Inc., San Diego.
(39) Vagin, A., and Teplyakov, A. (1997) MOLREP: An automated program for molecular replacement. *J. Appl. Crystallogr. 30*, 1022−1025.
(40) Adams, P. D., Afonine, P. V., Bunkoczi, G., Chen, V. B., Davis, I. W., Echols, N., Headd, J. J., Hung, L. W., Kapral, G. J., Grosse-Kunstleve, R. W., McCoy, A. J., Moriarty, N. W., Oeffner, R., Read, R. J., Richardson, D. C., Richardson, J. S., Terwilliger, T. C., and Zwart, P. H. (2010) PHENIX: A comprehensive Python-based system for macromolecular structure solution. *Acta Crystallogr. D66*, 213−221.
(41) Weis, D. D., Engen, J. R., and Kass, I. J. (2006) Semi-automated data processing of hydrogen exchange mass spectra using HX-Express. *J. Am. Soc. Mass Spectrom. 17*, 1700−1703.
(42) Agazie, Y. M., and Hayman, M. J. (2003) Molecular mechanism for a role of SHP2 in epidermal growth factor receptor signaling. *Mol. Cell. Biol. 23*, 7875−7886.
(43) Jarvis, L. A., Toering, S. J., Simon, M. A., Krasnow, M. A., and Smith-Bolton, R. K. (2006) Sprouty proteins are in vivo targets of Corkscrew/SHP-2 tyrosine phosphatases. *Development 133*, 1133−1142.
(44) Ren, Y., Meng, S., Mei, L., Zhao, Z. J., Jove, R., and Wu, J. (2004) Roles of Gab1 and SHP2 in paxillin tyrosine dephosphorylation and Src activation in response to epidermal growth factor. *J. Biol. Chem. 279*, 8497−8505.
(45) Edouard, T., Combier, J. P., Nédélec, A., Bel-Vialar, S., Métrich, M., Conte-Auriol, F., Lyonnet, S., Parfait, B., Tauber, M., Salles, J. P., Lezoualc'h, F., Yart, A., and Raynal, P. (2010) Functional effects of

PTPN11 (SHP2) mutations causing LEOPARD syndrome on epidermal growth factor-induced phosphoinositide 3-kinase/AKT/glycogen synthase kinase 3β signaling. *Mol. Cell. Biol. 30*, 2498−2507.
(46) Zhang, Z.-Y. (2003) Mechanistic studies on protein tyrosine phosphatases. *Prog. Nucleic Acid Res. Mol. Biol. 73*, 171−220.
(47) Guan, K. L., and Dixon, J. E. (1991) Evidence for protein-tyrosine phosphatase catalysis proceeding via a cysteine-phosphate intermediate. *J. Biol. Chem. 266*, 17026−17030.
(48) Cho, H., Krishnaraj, R., Kitas, E., Bannwarth, W., Walsh, C. T., and Anderson, K. S. (1992) Isolation and structural elucidation of a novel phosphocysteine intermediate in the LAR protein tyrosine phosphatase enzymatic pathway. *J. Am. Chem. Soc. 114*, 7296−7298.
(49) Zhang, Z.-Y., Wang, Y., and Dixon, J. E. (1994) Dissecting the catalytic mechanism of protein tyrosine phosphatases. *Proc. Natl. Acad. Sci. U.S.A. 91*, 1624−1627.
(50) Hengge, A. C., Sowa, G., Wu, L., and Zhang, Z.-Y. (1995) Nature of the Transition State of the Protein-Tyrosine Phosphatase-Catalyzed Reaction. *Biochemistry 34*, 13982−13987.
(51) Wu, L., and Zhang, Z.-Y. (1996) Probing the function of Asp128 in the low molecular weight protein-tyrosine phosphatase catalyzed reaction. A pre-steady-state and steady-state kinetic investigation. *Biochemistry 35*, 5426−5434.
(52) Lohse, D. L., Denu, J. M., Santoro, N., and Dixon, J. E. (1997) Roles of aspartic acid-181 and serine-222 in intermediate formation and hydrolysis of the mammalian protein-tyrosine-phosphatase PTP1. *Biochemistry 36*, 4568−4575.
(53) Zhao, Y., Wu, L., Noh, S. J., Guan, K. L., and Zhang, Z.-Y. (1998) Altering the nucleophile specificity of a protein-tyrosine phosphatase-catalyzed reaction: Probing the function of the invariant glutamine residues. *J. Biol. Chem. 273*, 5484−5492.
(54) Pannifer, A. D., Flint, A. J., Tonks, N. K., and Barford, D. (1998) Visualization of the cysteinyl-phosphate intermediate of a protein-tyrosine phosphatase by X-ray crystallography. *J. Biol. Chem. 273*, 10454−10462.
(55) Zhang, Z.-Y., Wang, Y., Wu, L., Fauman, E., Stuckey, J. A., Schubert, H. L., Saper, M. A., and Dixon, J. E. (1994) The $Cys(X)_5Arg$ catalytic motif in phosphoester hydrolysis. *Biochemistry 33*, 15266−15270.
(56) Zhang, Y.-L., Hollfelder, F., Gordon, S. J., Chen, L., Keng, Y.-F., Wu, L., Herschlag, D., and Zhang, Z.-Y. (1999) Impaired transition state complementarity in the hydrolysis of *O*-arylphosphorothioates by protein-tyrosine phosphatases. *Biochemistry 38*, 12111−12123.
(57) Hoff, R. H., Wu, L., Zhou, B., Zhang, Z.-Y., and Hengge, A. C. (1999) Does positive charge at the active site of a phosphatase cause a change in mechanism? The effect of the conserved arginine on the transition state for enzymatic phosphoryl transfer in the protein-tyrosine phosphatase from *Yersinia*. *J. Am. Chem. Soc. 121*, 9514−9521.
(58) Alhambra, C., Wu, L., Zhang, Z.-Y., and Gao, J. (1998) Walden-Inversion Enforced Transition State Stabilization in a Protein Tyrosine Phosphatase. *J. Am. Chem. Soc. 120*, 3858−3866.
(59) Jia, Z. C., Barford, D., Flint, A. J., and Tonks, N. K. (1995) Structural basis for phosphotyrosine peptide recognition by protein tyrosine phosphatase 1B. *Science 268*, 1754−1758.
(60) Brandao, T. A. S., Hengge, A. C., and Johnson, S. J. (2010) Insights into the Reaction of Protein-tyrosine Phosphatase 1B Crystal Structures for Transition State Analogs of Both Catalytic Steps. *J. Biol. Chem. 285*, 15874−15883.
(61) Hoofnagle, A. N., Resing, K. A., and Ahn, N. G. (2003) Protein analysis by hydrogen exchange mass spectrometry. *Annu. Rev. Biophys. Biomol. Struct. 32*, 1−25.
(62) Wales, T. E., and Engen, J. R. (2006) Hydrogen exchange mass spectrometry for the analysis of protein dynamics. *Mass Spectrom. Rev. 25*, 158−170.
(63) Holgado-Madruga, M., Emlet, D. R., Moscatello, D. K., Godwin, A. K., and Wong, A. J. (1996) A Grb2-associated docking protein in EGF- and insulin-receptor signaling. *Nature 379*, 560−564.
(64) Cunnick, J. M., Dorsey, J. F., Munoz-Antonia, T., Mei, L., and Wu, J. (2000) Requirement of SHP2 binding to Grb2-associated binder-1 for mitogen-activated protein kinase activation in response to lysophosphatidic acid and epidermal growth factor. *J. Biol. Chem. 275*, 13842−13848.
(65) Cunnick, J. M., Mei, L., Doupnik, C. A., and Wu, J. (2001) Phosphotyrosines 627 and 659 of Gab1 constitute a bisphosphoryl tyrosine-based activation motif (BTAM) conferring binding and activation of SHP2. *J. Biol. Chem. 276*, 24380−24387.
(66) Qu, C. K., Yu, W. M., Azzarelli, B., and Feng, G. S. (1999) Genetic evidence that Shp-2 tyrosine phosphatase is a signal enhancer of the epidermal growth factor receptor in mammals. *Proc. Natl. Acad. Sci. U.S.A. 96*, 8528−8533.
(67) Maroun, C. R., Naujokas, M. A., Holgado-Madruga, M., Wong, A. J., and Park, M. (2000) The tyrosine phosphatase SHP-2 is required for sustained activation of extracellular signal-regulated kinase and epithelial morphogenesis downstream from the Met receptor tyrosine kinase. *Mol. Cell. Biol. 20*, 8513−8525.
(68) Schaeper, U., Gehring, N. H., Fuchs, K. P., Sachs, M., Kempkes, B., and Birchmeier, W. (2000) Coupling of Gab1 to c-Met, Grb2, and Shp2 mediates biological responses. *J. Cell Biol. 149*, 1419−1432.
(69) Carcavilla, A., Santome, J. L., Pinto, I., Sanchez-Pozo, J., Guillen-Navarro, E., Martin-Frias, M., Lapunzin, P., and Ezquieta, B. (2013) LEOPARD Syndrome: A Variant of Noonan Syndrome Strongly Associated With Hypertrophic Cardiomyopathy. *Rev. Esp. Cardiol. 66*, 350−356.
(70) Tidyman, W. E., and Rauen, K. A. (2009) The RASopathies: Developmental syndromes of Ras/MAPK pathway dysregulation. *Curr. Opin. Genet. Dev. 19*, 230−236.
(71) Edouard, T., Montagner, A., Dance, M., Conte, F., Yart, A., Parfait, B., Tauber, M., Salles, J. P., and Raynal, P. (2007) How do Shp2 mutations that oppositely influence its biochemical activity result in syndromes with overlapping symptoms? *Cell. Mol. Life Sci. 64*, 1585−1590.
(72) Carta, C., Pantaleoni, F., Bocchinfuso, G., Stella, L., Vasta, I., Sarkozy, A., Digilio, C., Palleschi, A., Pizzuti, A., Grammatico, P., Zampino, G., Dallapiccola, B., Gelb, B. D., and Tartaglia, M. (2006) Germline missense mutations affecting KRAS isoform B are associated with a severe Noonan syndrome phenotype. *Am. J. Hum. Genet. 79*, 129−135.
(73) Schubbert, S., Zenker, M., Rowe, S. L., Boll, S. B., Klein, C., Bollag, G., van der Burgt, I., Musante, L., Kalscheuer, V., Wehner, L. E., Nguyen, H., West, B., Zhang, K. Y. J., Sistermans, E., Rauch, A., Niemeyer, C. M., Shannon, K., and Kratz, C. P. (2006) Germline KRAS mutations cause Noonan syndrome. *Nat. Genet. 38*, 331−336.
(74) Roberts, A. E., Araki, T., Swanson, K. D., Montgomery, K. T., Schiripo, T. A., Joshi, V. A., Li, L., Yassin, Y., Tamburino, A. M., Neel, B. G., and Kucherlapati, R. S. (2007) Germline gain-of-function mutations in SOS1 cause Noonan syndrome. *Nat. Genet. 39*, 70−74.
(75) Tartaglia, M., Pennacchio, L. A., Zhao, C., Yadav, K. K., Fodale, V., Sarkozy, A., Pandit, B., Oishi, K., Martinelli, S., Schackwitz, W., Ustaszewska, A., Martin, J., Bristow, J., Carta, C., Lepri, F., Neri, C., Vasta, I., Gibson, K., Curry, C. J., Siguero, J. P. L., Digilio, M. C., Zampino, G., Dallapiccola, B., Bar-Sagi, D., and Gelb, B. D. (2007) Gain-of-function SOS1 mutations cause a distinctive form of Noonan syndrome. *Nat. Genet. 39*, 75−79.
(76) Pandit, B., Sarkozy, A., Pennacchio, L. A., Carta, C., Oishi, K., Martinelli, S., Pogna, E. A., Schackwitz, W., Ustaszewska, A., Landstrom, A., Bos, J. M., Ommen, S. R., Esposito, G., Lepri, F., Faul, C., Mundel, P., Siguero, J. P. L., Tenconi, R., Selicorni, A., Rossi, C., Mazzanti, L., Torrente, I., Marino, B., Digilio, M. C., Zampino, G., Ackerman, M. J., Dallapiccola, B., Tartaglia, M., and Gelb, B. D. (2007) Gain-of-function RAF1 mutations cause Noonan and LEOPARD syndromes with hypertrophic cardiomyopathy. *Nat. Genet. 39*, 1007−1012.
(77) Razzaque, M. A., Nishizawa, T., Komoike, Y., Yagi, H., Furutani, M., Amo, R., Kamisago, M., Momma, K., Katayama, H., Nakagawa, M., Fujiwara, Y., Matsushima, M., Mizuno, K., Tokuyama, M., Hirota, H., Muneuchi, J., Higashinakagawa, T., and Matsuoka, R. (2007) Germline gain-of-function mutations in RAF1 cause Noonan syndrome. *Nat. Genet. 39*, 1013−1017.

(78) Sarkozy, A., Carta, C., Moretti, S., Zampino, G., Digilio, M. C., Pantaleoni, F., Scioletti, A. P., Esposito, G., Cordeddu, V., Lepri, F., Petrangeli, V., Dentici, M. L., Mancini, G. M. S., Selicorni, A., Rossi, C., Mazzanti, L., Marino, B., Ferrero, G. B., Silengo, M. C., Memo, L., Stanzial, F., Faravelli, F., Stuppia, L., Puxeddu, E., Gelb, B. D., Dallapiccola, B., and Tartaglia, M. (2009) Germline BRAF Mutations in Noonan, LEOPARD, and Cardiofaciocutaneous Syndromes: Molecular Diversity and Associated Phenotypic Spectrum. *Hum. Mutat. 30*, 695−702.

(79) Cirstea, I. C., Kutsche, K., Dvorsky, R., Gremer, L., Carta, C., Horn, D., Roberts, A. E., Lepri, F., Merbitz-Zahradnik, T., Konig, R., Kratz, C. P., Pantaleoni, F., Dentici, M. L., Joshi, V. A., Kucherlapati, R. S., Mazzanti, L., Mundlos, S., Patton, M. A., Silengo, M. C., Rossi, C., Zampino, G., Digilio, C., Stuppia, L., Seemanova, E., Pennacchio, L. A., Gelb, B. D., Dallapiccola, B., Wittinghofer, A., Ahmadian, M. R., Tartaglia, M., and Zenker, M. (2010) A restricted spectrum of NRAS mutations causes Noonan syndrome. *Nat. Genet. 42*, 27−29.

(80) Aoki, Y., Niihori, T., Kawame, H., Kurosawa, K., Ohashi, H., Tanaka, Y., Filocamo, M., Kato, K., Suzuki, Y., Kure, S., and Matsubara, Y. (2005) Germline mutations in HRAS proto-oncogene cause Costello syndrome. *Nat. Genet. 37*, 1038−1040.

(81) Niihori, T., Aoki, Y., Narumi, Y., Neri, G., Cavé, H., Verloes, A., Okamoto, N., Hennekam, R. C., Gillessen-Kaesbach, G., Wieczorek, D., Kavamura, M. I., Kurosawa, K., Ohashi, H., Wilson, L., Heron, D., Bonneau, D., Corona, G., Kaname, T., Naritomi, K., Baumann, C., Matsumoto, N., Kato, K., Kure, S., and Matsubara, Y. (2006) Germline KRAS and BRAF mutations in cardio-facio-cutaneous syndrome. *Nat. Genet. 38*, 294−296.

(82) Rodriguez-Viciana, P., Tetsu, O., Tidyman, W. E., Estep, A. L., Conger, B. A., Cruz, M. S., McCormick, F., and Rauen, K. A. (2006) Germline mutations in genes within the MAPK pathway cause cardio-facio-cutaneous syndrome. *Science 311*, 1287−1290.

(83) Gelb, B. D., and Tartaglia, M. (2006) Noonan syndrome and related disorders: Dysregulated RAS-mitogen activated protein kinase signal transduction. *Hum. Mol. Genet. 15*, R220−R226.

(84) Stewart, R. A., Sanda, T., Widlund, H. R., Zhu, S. Z., Swanson, K. D., Hurley, A. D., Bentires-Alj, M., Fisher, D. E., Kontaridis, M. I., Look, A. T., and Neel, B. G. (2010) Phosphatase-Dependent and -Independent Functions of Shp2 in Neural Crest Cells Underlie LEOPARD Syndrome Pathogenesis. *Dev. Cell 18*, 750−762.

(85) Marin, T. M., Keith, K., Davies, B., Conner, D. A., Guha, P., Kalaitzidis, D., Wu, X., Lauriol, J., Wang, B., Bauer, M., Bronson, R., Franchini, K. G., Neel, B. G., and Kontaridis, M. I. (2011) Rapamycin reverses hypertrophic cardiomyopathy in a mouse model of LEOPARD syndrome-associated PTPN11 mutation. *J. Clin. Invest. 121*, 1026−1043.

(86) Oishi, K., Zhang, H., Gault, W. J., Wang, C. J., Tan, C. C., Kim, I. K., Ying, H. W., Rahman, T., Pica, N., Tartaglia, M., Mlodzik, M., and Gelb, B. D. (2009) Phosphatase-defective LEOPARD syndrome mutations in PTPN11 gene have gain-of-function effects during *Drosophila* development. *Hum. Mol. Genet. 18*, 193−201.

(87) Carvajal-Vergara, X., Sevilla, A., D'Souza, S. L., Ang, Y. S., Schaniel, C., Lee, D. F., Yang, L., Kaplan, A. D., Adler, E. D., Rozov, R., Ge, Y. C., Cohen, N., Edelmann, L. J., Chang, B., Waghray, A., Su, J., Pardo, S., Lichtenbelt, K. D., Tartaglia, M., Gelb, B. D., and Lemischka, I. R. (2010) Patient-specific induced pluripotent stem-cell-derived models of LEOPARD syndrome. *Nature 465*, 808−812.

(88) Feng, G. S., Hui, C. C., and Pawson, T. (1993) SH2-containing phosphotyrosine phosphatase as a target of protein-tyrosine kinases. *Science 259*, 1607−1611.

(89) Vogel, W., Lammers, R., Huang, J. T., and Ullrich, A. (1993) Activation of a phosphotyrosine phosphatase by tyrosine phosphorylation. *Science 259*, 1611−1614.

(90) Lu, W., Gong, D. Q., Bar-Sagi, D., and Cole, P. A. (2001) Site-specific incorporation of a phosphotyrosine mimetic reveals a role for tyrosine phosphorylation of SHP-2 in cell signaling. *Mol. Cell 8*, 759−769.